IEEE Access
Multidisciplinary | Rapid Review | Open Access Journal

Received September 20, 2021, accepted October 4, 2021, date of publication October 6, 2021, date of current version October 13, 2021.

Digital Object Identifier 10.1109/ACCESS.2021.3118377

Secure and Fast Image Encryption Algorithm Using Hyper-Chaos-Based Key Generator and Vector Operation

BIN GE[1], XU CHEN[2], GANG CHEN[2], AND ZHIHUA SHEN[1]
[1]Electronic Information Engineering College, Nantong Vocational University, Nantong 226007, China
[2]Institute of Semiconductors, Chinese Academy of Sciences, Beijing 100083, China

Corresponding author: Bin Ge (bge@mail.ntvu.edu.cn)

This work was supported in part by the National Natural Science Foundation of China under Grant U1936106, Grant U19A2080, and Grant 62004108; in part by the Natural Science Foundation for Universities of Jiangsu Province under Grant 20KJD510001; in part by Qing Lan Project of Colleges and Universities in Jiangsu Province under Grant 苏教师函(2020) 10 号; and in part by Nantong Science and Technology Plan Project under Grant JC2021036.

ABSTRACT To protect image data privacy, a secure and fast image encryption algorithm using hyper-chaos based key generator and vector operation is proposed. Firstly, we introduce a novel post-process method to create a key matrix for significantly reducing the iterations of the hyperchaotic system from $W \times H/4$ to $2W$ for an image size of $W \times H$. And within the post-process, a random selector driven by the piecewise linear chaotic map ensures the good randomness and unpredictability of the generated key matrix. Secondly, the vector operation is employed to accelerate the cipher block chaining based diffusion process, so the plain image can be parallel encrypted row by row and column by column with high efficiency. Thirdly, we utilize a Logistic map to quickly produce an initial vector for the vectorized diffusion process. Finally, the proposed algorithm is evaluated by some common security and performance tests. Experimental results show that the cipher image can pass all tests of NIST SP 800-22 with P-values $\gg 0.01$, its correlation coefficient between pixels is close to 0, and the entropy is greater than 7.999. Combined with other results of security tests, we can safely conclude that the proposed image encryption algorithm provides adequate protection against statistical, brute-force, chosen-plaintext, and other common types of attacks. In addition, the time complexity is in the order of $\boldsymbol{O}(W + H)$ and the average encryption time of 512×512 images is only 0.023s. The results indicate that our algorithm with high security and fast speed can meet the requirements of real-time confidential transmission of massive image data.

INDEX TERMS Image encryption, hyperchaotic system, key generator, vector operation.

I. INTRODUCTION

With the vigorous development of information technology and online social media, digital images have become part of our daily living [1], [2]. However, numerous images are produced and transmitted daily without adequate protection over the Internet [3]–[5]. Meanwhile, with the gradual popularization of IoT, devices are creating more and more digital images at an alarming rate, securing image data in complex open transmission channels has become a common concern [6]–[8]. At present, encryption and watermarking techniques have become the two major thrusts of image security research. But the small capacity of data hiding makes the watermarking technique more suitable to protect the copyright of digital images [9], [10]. Certainly, the encryption technique makes it possible for us to transmit massive image data without leaking any useful information whether in wireless or wired communications [7]. Although block ciphers, such as 3DES and AES, are commonly adopted [11], [12], extensive practical results [13], [14] indicate that these algorithms designed for textual data cannot effectively encrypt images partially given the low processing speed due to the large amount and high redundancy of image data [15]. Hence, many novel image orientated encryption algorithms have been proposed [16]–[19] with chaos-based image encryption being the most representative approach.

In 1989, Matthews [20] proposed the first stream cipher algorithm using a Logistic map. Since the development

The associate editor coordinating the review of this manuscript and approving it for publication was Ludovico Minati.

of chaos control and chaos synchronization in 1990 [21], the application of chaotic systems to cryptosystems has been increasingly explored. In 1998, Fridrich [22] used a two-dimensional Baker's map to develop a common permutation-diffusion structure to fully hide the relationship between a plain image and its corresponding cipher image. Although various techniques have been introduced to enhance the algorithm security [23]–[26], some inevitable risks, such as the small key space, low linear complexity, and short periodic orbit [27], [28], limit the application of low-dimensional chaotic map to image encryption algorithms. However, the theory of hyper-chaos may be helpful to overcome these limitations [29]–[32]. In general, a hyperchaotic system with more than two positive Lyapunov exponents can exhibit more complex attractors, higher unpredictability, and stronger randomness. Moreover, it typically needs more than four state values for iteration, naturally providing a large key space for the corresponding cryptosystem.

In 2008, Gao and Chen [33] proposed the first hyperchaotic image encryption algorithm, but it was vulnerable to the chosen-plaintext attacks [34] because its key sequence was independent of the plain image. Thereafter, Li *et al.* [35] proposed a plaintext-related image encryption algorithm that obtains the initial values of the hyperchaotic system from nine original pixels. However, the sensitivity to variations in other pixels by the application of one-round diffusion was inadequate. A more secure approach should adopt at least two-round cipher block chaining (CBC) based diffusion for the cipher image to relate to every original pixel. But on the other hand, the CBC based diffusion process was serial in common, which led to a practical problem of low encryption speed [36], [37]. Thus, in 2017, Yuan *et al.* [38] introduced a pixel classification method to parallelize the CBC based diffusion process. However, the insufficient parallelism degree and the usage of rotation resulted in an unsatisfactory efficiency. Then, in 2019, Çavuşoğlu *et al.* [39] depended on the multi-thread technique to accelerate encryption after dividing the plain image into several subsequences, but the lack of diffusion between threads would cause security issues. In 2020, Zhou and Wnag [40] converted the original image into multiple 4×4 blocks to encrypt 16 pixels in parallel using a key mask and XOR operation. But only one-round diffusion rendered the proposed algorithm vulnerable to the chosen-plaintext attack and chosen-ciphertext attack. Also in 2020, Zhao and Ren [41] presented a highly parallelized algorithm by extending the CBC technique from pixel level to row level, the diffusion process in column remained serialized, and the overall diffusion process could only let pixel information influence its lower-right corner. In general, there is still no appropriate image encryption algorithm to balance security and speed.

Moreover, few studies are available on the time consumption of hyper-chaos based key generators, but it is quite important to improve the efficiency of the image encryption algorithm. On closer inspection, we find that the key generation process even takes longer than the diffusion process [38]–[41]. In order to solve the above problems, we propose a secure and fast image encryption algorithm using hyper-chaos based key generator and vector operation. Firstly, the key generation process is redesigned to produce a key matrix according to the size of the plain image. By applying a post-process method, the number of iterations in the hyperchaotic system can be substantially reduced from $W \times H/4$ to $2W$. Taking the two-dimensional structure of the image into consideration, we introduce the vector operation into the CBC based diffusion process, then pixels on a row or column can be encrypted in parallel. Furthermore, the cipher image is highly sensitive to every pixel change through four-round chained diffusion in the vertical direction and horizontal direction. Detailed results and analyses of the security and efficiency performance show that the proposed algorithm can provide fast encryption and can resist various cryptographic attacks such as statistical, brute-force, and chosen-plaintext attacks.

Briefly, the main contributions of this paper can be summarized as follows.

(1) Based on a hyperchaotic system and vector operation, we propose a novel image encryption algorithm that can provide high security protection and fast encryption speed for massive image data transmission on the public channel.

(2) A novel post-process method for the hyper-chaos based key generator is presented. By using bitwise XOR operation and circular shift operation on key stream, a $W \times H$ key matrix can be obtained with a 4D hyperchaotic system only iterating $2W$ times. More importantly, a random selector within the post-process guarantees the randomness and unpredictability of the key matrix.

(3) We utilize the vector operation to accelerate the CBC based diffusion process. Hence, the plain image can be encrypted by row in the vertical direction and by column in the horizontal direction. Moreover, the update of initial vector between two diffusion rounds during the four-round encryption process ensures adequate diffusion, and thus even minor changes of any pixel can significantly influence the results of the encryption.

The remainder of this paper is organized as follows. Section II presents the preliminaries for this study. In Section III, we introduce the proposed image encryption algorithm. In Section IV, we report and analyze the experimental results of the proposed algorithm. In Section V, we further test the proposed algorithm on color images. Finally, we draw conclusions in Section VI.

II. PRELIMINARIES

In this section, all the chaotic systems for constructing the proposed image encryption algorithm are presented, and the mechanism of vector operation is also described.

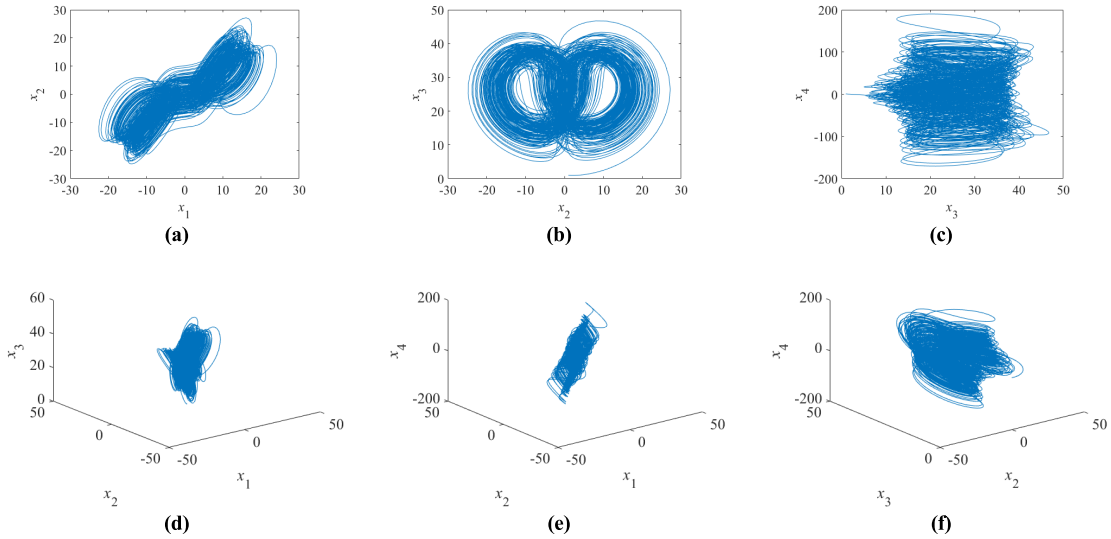

FIGURE 1. Attractors of HCLS on (a) x_1–x_2, (b) x_2–x_3, and (c) x_3–x_4 planes and (d) x_1–x_2–x_3, (e) x_1–x_2–x_4, and (f) x_2–x_3–x_4 spaces.

A. HYPERCHAOTIC LORENZ SYSTEM

Nowadays, various new types of hyperchaotic systems [42]–[45] have emerged. But as one of the most often used hyperchaotic systems to construct secure image encryption algorithms, the hyperchaotic Lorenz system (HCLS) has been proved to have good inherent randomness, high initial sensitivity, and large key space [46], [47]. Moreover, many observations have verified that HCLS keeps chaos character with long period in the digital system [29], [33], [35]–[37], [46], [47]. In this study, we add a nonlinear controller $\dot{x}_4 = -x_2x_3 + dx_4$ on the original Lorenz system [47], then the HCLS equation is given by

$$\begin{cases} \dot{x}_1 = a(x_2 - x_1) + x_4 \\ \dot{x}_2 = cx_1 - x_2 - x_1x_3 \\ \dot{x}_3 = x_1x_2 - bx_3 \\ \dot{x}_4 = -x_2x_3 + dx_4 \end{cases} \tag{1}$$

where a, b, c, and d are control parameters of HCLS.

For $a = 10$, $b = 8/3$, $c = 28$, and $d = -1$, the system contains two positive Lyapunov exponents [48]: $\mathrm{LE}_1 = 0.3381$ and $\mathrm{LE}_2 = 0.1586$. Hence, the system evolves into a hyperchaotic state and can generate an extremely complex and dense motion trajectory, as shown in Fig. 1. Therefore, we can rely on the HCLS to implement a secure pseudorandom number generator with a long period and high linear complexity.

B. PIECEWISE LINEAR CHAOTIC MAP

The piecewise linear chaotic map (PWLCM) [49] is given by

$$y(i+1) = F_p(y(i)) = \begin{cases} y(i)/p, & 0 < y(i) < p \\ (y(i) - p)/(0.5 - p), & p \le y(i) < 0.5 \\ F_p(1 - y(i)), & 0.5 \le y(i) < 1 \end{cases} \tag{2}$$

where p is a control parameter and $y(i) \in (0,1)$.

The PWLCM evolves into a chaotic state, when p is in the range of 0 and 0.5. In this paper, we let $p = 0.25$ for the research. Since the PWLCM has a very simple structure, and can rapidly generate a sequence of uniform distribution, we employ it in a fast random selector for post-processing the pseudorandom numbers to obtain a secure key matrix according to the size of the plain image.

C. LOGISTIC MAP

The Logistic map (LM) [50] is a famous one-dimensional chaotic system given by

$$z(i+1) = \mu z(i)(1 - z(i)) \tag{3}$$

where μ is the control parameter that must be in the range of 3.56 and 4 for chaotic behavior [51].

In this study, we utilize LM, and set $\mu = 4$ to get the largest Lyapunov exponent, as a producer to quickly generate an initial vector for the vectorized CBC based diffusion process.

D. VECTOR OPERATION

A vector operation refers to the simultaneous application of an operation to a set of values. Thus, it allows to operate on aggregates of data without resorting to loops to handle individual scalar operations. Nowadays most CPUs combined with a modern programming language and single instruction multiple data extension (SIMD) can accelerate the program execution speed by implicit parallelization using vector operation.

Suppose $i = 1, 2, \ldots, n-1, n$, $\boldsymbol{V}_r^1 = \{v_r^1(i)\}$, $\boldsymbol{V}_r^2 = \{v_r^2(i)\}$ are two row vectors with length n, $\boldsymbol{V}_c^1 = \{v_c^1(i)\}^{\mathrm{T}}$, $\boldsymbol{V}_c^2 = \{v_c^2(i)\}^{\mathrm{T}}$ are two column vectors with height n, and s is a scalar. We define function vec_opr() as a kind of operation between two vectors (or between a vector and a scalar) and function opr() as a kind of operation between two scalars,

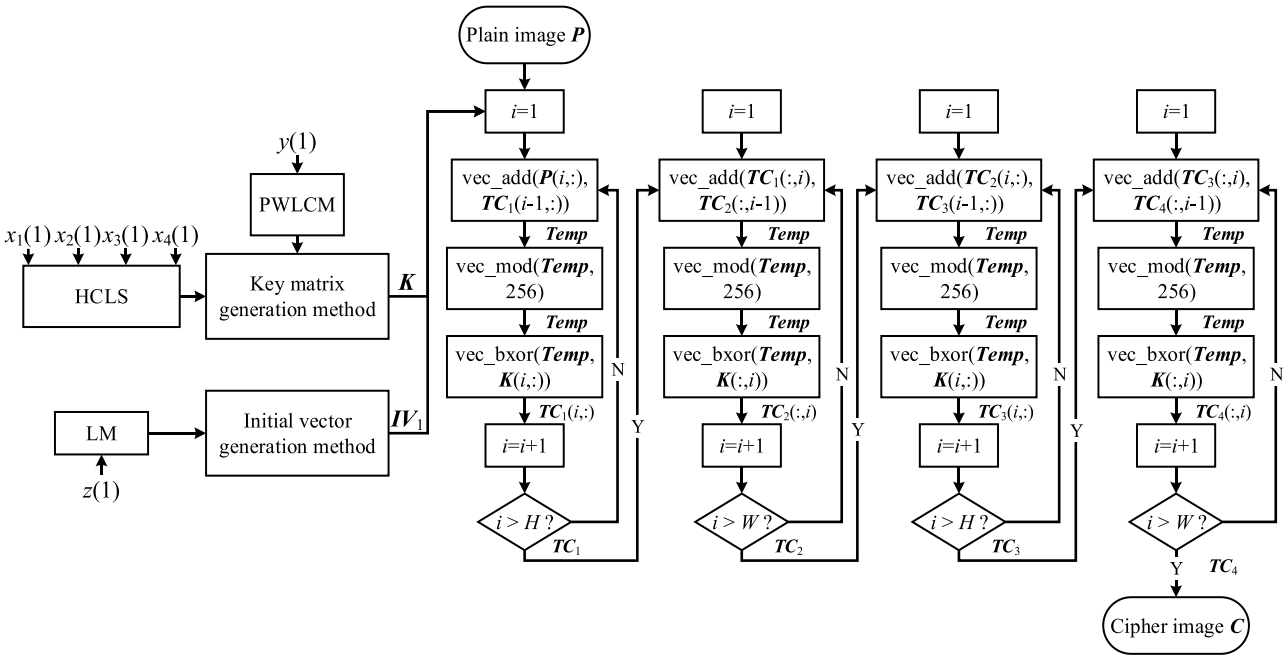

FIGURE 2. Flow diagram of the proposed encryption algorithm.

then the vector operations are described in Eq. (4). At present, SIMD has evolved from SSE 128 bits to AVX 512 bits [52] endowing vector operations with a more powerful parallel computing ability. Furthermore, vectorization is requisite to implement algorithms in parallel computing platforms, such as the graphics processing unit (GPU) and the field-programmable gate array (FPGA). As digital image data are stored in matrix form, many image processing algorithms have been vectorized to improve the operating efficiency [53], [54].

$$\begin{cases} \text{vec\_opr}(\boldsymbol{V}_r^1, V_r^2\} = \{\text{opr}(v_r^1(i), v_r^2(i))\} \\ \text{vec\_opr}(\boldsymbol{V}_c^1, V_c^2\} = \{\text{opr}(v_c^1(i), v_c^2(i))\}^{\mathrm{T}} \\ \text{vec\_opr}(\boldsymbol{V}_r^1, s\} = \{\text{opr}(v_r^1(i), s)\} \\ \text{vec\_opr}(\boldsymbol{V}_c^1, s\} = \{\text{opr}(v_c^1(i), s)\}^{\mathrm{T}} \\ i = 1, 2, \ldots, n-1, n \end{cases} \tag{4}$$

III. THE PROPOSED SECURE AND FAST IMAGE ENCRYPTION ALGORITHM

In this section, the proposed image encryption algorithm is detailed regarding a key matrix generation method, an initial vector generation method, and a four-round vectorized diffusion method. The flow diagram of our algorithm is shown in Fig. 2, where W and H are the width and height of the plain image respectively, functions vec_add(), vec_mod(), and vec_bxor() represent the vectorized operations of addition, modulus, and bitwise XOR (bitxor). It must be noted that, for the sake of simplification, although we use common operations in the following subsections to calculate vectors (or a vector and a scalar), they represent the vectorized operations.

A. THE KEY MATRIX GENERATION METHOD

To obtain the key stream for encrypting an image, the real-valued chaotic sequence must be converted into an integer sequence. The general process to get the key stream is shown in Fig. 3. Thus the HCLS must perform at least $WH/4$ iterations to obtain a key stream with enough length for encryption.

However, the high complexity of the hyperchaotic system imposes a tradeoff between security and efficiency in a cryptosystem. By introducing a key schedule method to post-process the key stream, a $W \times H$ key matrix can be quickly obtained, as shown in Fig. 4, with the HCLS only iterating $2W$ times.

Then, the Algorithm and descriptions of the key matrix generation method are detailed below:

Step 1: Input $x_1(1)$, $x_2(1)$, $x_3(1)$, $x_4(1)$, then use the fourth-order Runge-Kutta method to iterate the HCLS pre_1 times to overcome the transient effect.

Step 2: Initialize an empty sequence $\boldsymbol{B}$ of length $8W$.

Step 3: Continue to iterate HCLS $2W$ times and fill new state values into $\boldsymbol{B}$.

Step 4: Transform the real-valued sequence $\boldsymbol{B}$ into an integer sequence $\boldsymbol{I}$.

Step 5: Input $y(1)$, then iterate PWLCM pre_2 times to overcome the transient effect.

Step 6: Initialize an empty sequence $\boldsymbol{S}$ of length $2H$.

Step 7: Continue to iterate the PWLCM $2H$ times and fill new state values into $\boldsymbol{S}$.

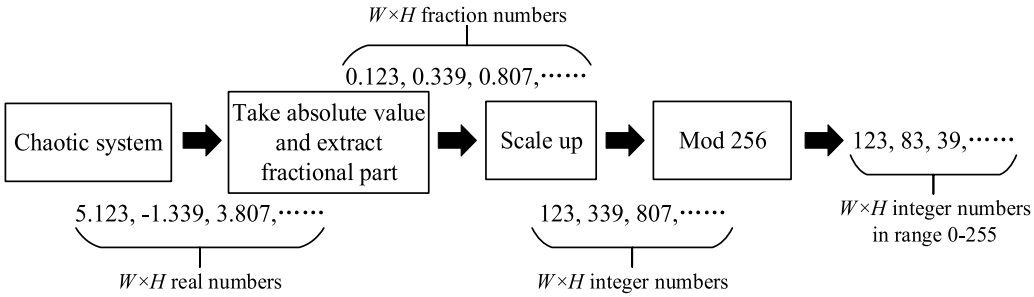

FIGURE 3. Flowchart of the general process to obtain the key stream.

Step 8: Transform the real-values sequence $\boldsymbol{S}$ into integer sequence $\boldsymbol{S}$'.

Step 9: Split $\boldsymbol{I}$ into eight subsequences of length W: $\boldsymbol{I}_1$–$\boldsymbol{I}_8$.

Step 10: Initialize an empty matrix $\boldsymbol{K}$ with the size of $W \times H$.

Step 11: Randomly choose $\boldsymbol{temp}_1$ from $\boldsymbol{I}_1$, $\boldsymbol{I}_2$, $\boldsymbol{I}_3$, $\boldsymbol{I}_4$, and $\boldsymbol{temp}_2$ from $\boldsymbol{I}_5$, $\boldsymbol{I}_6$, $\boldsymbol{I}_7$, $\boldsymbol{I}_8$.

Step 12: Apply bitxor operation between $\boldsymbol{temp}_1$ and $\boldsymbol{temp}_2$, and fill the result into $\boldsymbol{K}$, then update $\boldsymbol{I}_n$ using cyclic right shift (circshift) operation.

Step 13: Repeat *Step 11* and *Step 12* H times to obtain key matrix $\boldsymbol{K}$.

B. THE INITIAL VECTOR GENERATION METHOD

Similar to most CBC based diffusion algorithms, an initial vector is required in the proposed encryption algorithm to start diffusion. However, the initial vector for the vectorized diffusion process is longer than that for existing algorithms, consequently increasing the storage and transmission costs.

As the LM can rapidly produce many random numbers from few initial values, we use it to generate the required initial vector as follows:

Step 1: Input $z(1)$, then iterate the LM pre_3 times to overcome the transient effect.

Step 2: Initialize an empty sequence $\boldsymbol{V}$ with length of W.

Step 3: Continue to iterate the LM W times and fill new state values into $\boldsymbol{V}$.

Step 4: Transform real-valued sequence $\boldsymbol{V}$ into the initial vector $\boldsymbol{IV}_1$ consisting of integer numbers by

$$\boldsymbol{IV}_1 = \text{floor}(\boldsymbol{V} \times 10^{15}) \bmod 256 \tag{5}$$

C. THE FOUR-ROUND VECTORIZED DIFFUSION METHOD

Fig. 5 demonstrates how a 2×2 image is encrypted by the proposed four-round vectorized diffusion method, and the steps are detailed as follows.

Step 1: Input plain image $\boldsymbol{P}$, key matrix $\boldsymbol{K}$, and initial vectors $\boldsymbol{IV}_1$ as shown in Fig. 5(a).

Step 2: Use $\boldsymbol{K}$ for row-by-row encryption of $\boldsymbol{P}$ from top to bottom, as defined in Eq. (6). Let encrypted row to influence

Algorithm Key Matrix Generation Method

Input: Initial values $x_1(1), x_2(1), x_3(1), x_4(1)$, and pre_1 for HCLS; initial values $y(1)$, and pre_2 for PWLCM
Output: The key matrix $\boldsymbol{K}$
Put $x_1(1), x_2(1), x_3(1), x_4(1)$ into HCLS
for i from 1 to pre_1
  Iterate HCLS
  Drop the state values $x_1(i), x_2(i), x_3(i), x_4(i)$
end for
$\boldsymbol{B} \leftarrow$zeros(1, $8W$)
$x_1(1) \leftarrow x_1(pre_1+1)$; $x_2(1) \leftarrow x_2(pre_1+1)$;
$x_3(1) \leftarrow x_3(pre_1+1)$; $x_4(1) \leftarrow x_4(pre_1+1)$
Put new $x_1(1), x_2(1), x_3(1), x_4(1)$ into HCLS
for i from1 to $2W$
  iterate HCLS
  $\boldsymbol{B}(i) \leftarrow x_1(i+1)$
  $\boldsymbol{B}(i+2W+1) \leftarrow x_2(i+1)$
  $\boldsymbol{B}(i+4W+1) \leftarrow x_3(i+1)$
  $\boldsymbol{B}(i+6W+1) \leftarrow x_4(i+1)$
end for
$\boldsymbol{B}' \leftarrow$floor((abs($\boldsymbol{B}$)-floor(abs($\boldsymbol{B}$)))$\times 10^{15}$)mod256
Put $y(1)$ into PWLCM
for i from 1 to pre_2
  Iterate PWLCM
  Drop the state value $y(i)$
end for
$y(1) \leftarrow y(pre_2+1)$
Put new $y(1)$ into PWLCM
$\boldsymbol{B} \leftarrow$zeros(1, $2H$)
for i from 1to $2H$
  Iterate PWLCM
  $\boldsymbol{S}(i) \leftarrow y(i+1)$
end for
$\boldsymbol{S}' \leftarrow$floor($\boldsymbol{S} \times 10^{15}$)mod4+1
$\boldsymbol{I}_1 \leftarrow \boldsymbol{B}(1{:}W)$; $\boldsymbol{I}_2 \leftarrow \boldsymbol{B}(W+1{:}2W)$;
$\boldsymbol{I}_3 \leftarrow (2W+1{:}3W)$; $\boldsymbol{I}_4 \leftarrow \boldsymbol{B}(3W+1{:}4W)$;
$\boldsymbol{I}_5 \leftarrow (4W+1{:}5W)$; $\boldsymbol{I}_6(5W+1{:}6W)$;
$\boldsymbol{I}_7 \leftarrow (6W+1{:}7W)$; $\boldsymbol{I}_8 \leftarrow (7W+1{:}8W)$
$\boldsymbol{K} \leftarrow$zeros($W$, H)
for i from 1 to H
  $m \leftarrow \boldsymbol{S}'(2i\text{-}1)$; $n \leftarrow \boldsymbol{S}'(2i)+4$
  switch m
    case 1: $\boldsymbol{temp}_1 \leftarrow \boldsymbol{I}_1$
    case 2: $\boldsymbol{temp}_1 \leftarrow \boldsymbol{I}_2$
    case 3: $\boldsymbol{temp}_1 \leftarrow \boldsymbol{I}_3$
    case 4: $\boldsymbol{temp}_1 \leftarrow \boldsymbol{I}_4$
  end case
  switch n
    case 5: $\boldsymbol{temp}_2 \leftarrow \boldsymbol{I}_5$
    case 6: $\boldsymbol{temp}_2 \leftarrow \boldsymbol{I}_6$
    case 7: $\boldsymbol{temp}_2 \leftarrow \boldsymbol{I}_7$
    case 8: $\boldsymbol{temp}_2 \leftarrow \boldsymbol{I}_8$
  end case
  $\boldsymbol{K}(i,:) \leftarrow$bitxor($\boldsymbol{temp}_1$, $\boldsymbol{temp}_2$)
  $\boldsymbol{I}_n \leftarrow$circshift($\boldsymbol{temp}_2$,1)
end for

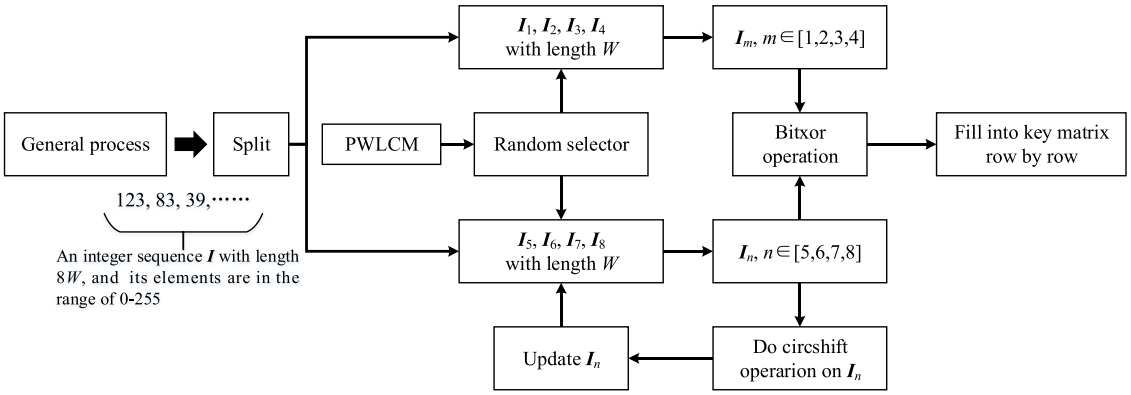

FIGURE 4. Flowchart of the post-process to obtain a key matrix.

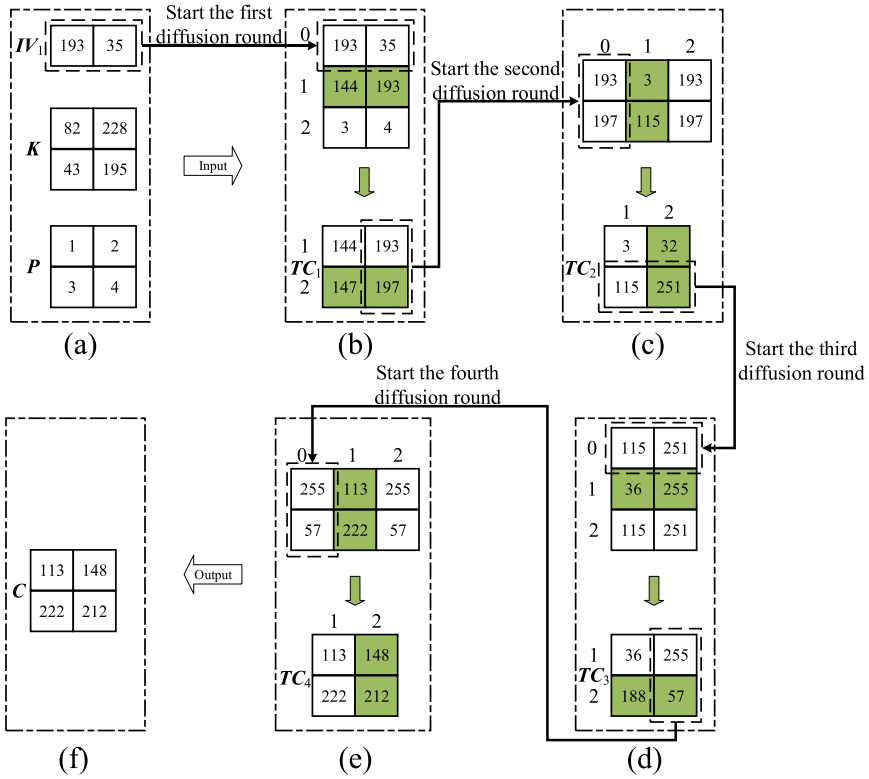

FIGURE 5. The diffusion process sketch map of a 2 × 2 image. (a) The input, (b) the first round of diffusion, (c) the second round of diffusion, (d) the third round of diffusion, (e) the fourth round of diffusion, (f) and the output.

the next row and $\boldsymbol{IV}_1$ to encrypt the first row. After the first round of diffusion, temporary cipher image $\boldsymbol{TC}_1$ is created, as illustrated in Fig. 5(b).

$$\begin{cases} \boldsymbol{TC}_1(0,:) = \boldsymbol{IV}_1 \\ \boldsymbol{temp} = (\boldsymbol{P}(i,:) + \boldsymbol{TC}_1(i-1,:)) \bmod 256 \\ \boldsymbol{TC}_1(i,:) = \text{bitxor}(\boldsymbol{K}(i,:), \boldsymbol{temp}) \\ i = 1, 2, \ldots, H-1, H \end{cases} \tag{6}$$

Step 3: Use $\boldsymbol{K}$ for column-by-column encryption of $\boldsymbol{TC}_1$ from left to right, as defined in Eq. (7). Let encrypted row to influence the next column and $\boldsymbol{IV}_2 = \boldsymbol{TC}_1(:, W)$ encrypt the first column. After the second round of diffusion, temporary cipher image $\boldsymbol{TC}_2$ is created, as illustrated in Fig. 5(c).

$$\begin{cases} \boldsymbol{TC}_2(:,0) = \boldsymbol{IV}_2 = \boldsymbol{TC}_1(:,W) \\ \boldsymbol{temp} = (\boldsymbol{TC}_1(:,i) + \boldsymbol{TC}_2(:,i-1)) \bmod 256 \\ \boldsymbol{TC}_2(:,i) = \text{bitxor}(\boldsymbol{K}(:,i), \boldsymbol{temp}) \\ i = 1, 2, \ldots, W-1, W \end{cases} \tag{7}$$

Step 4: Use $\boldsymbol{K}$ for row-by-row encryption of $\boldsymbol{TC}_3$ from top to bottom, as defined in Eq. (8), and $\boldsymbol{IV}_3 = \boldsymbol{TC}_2(H,:)$ to

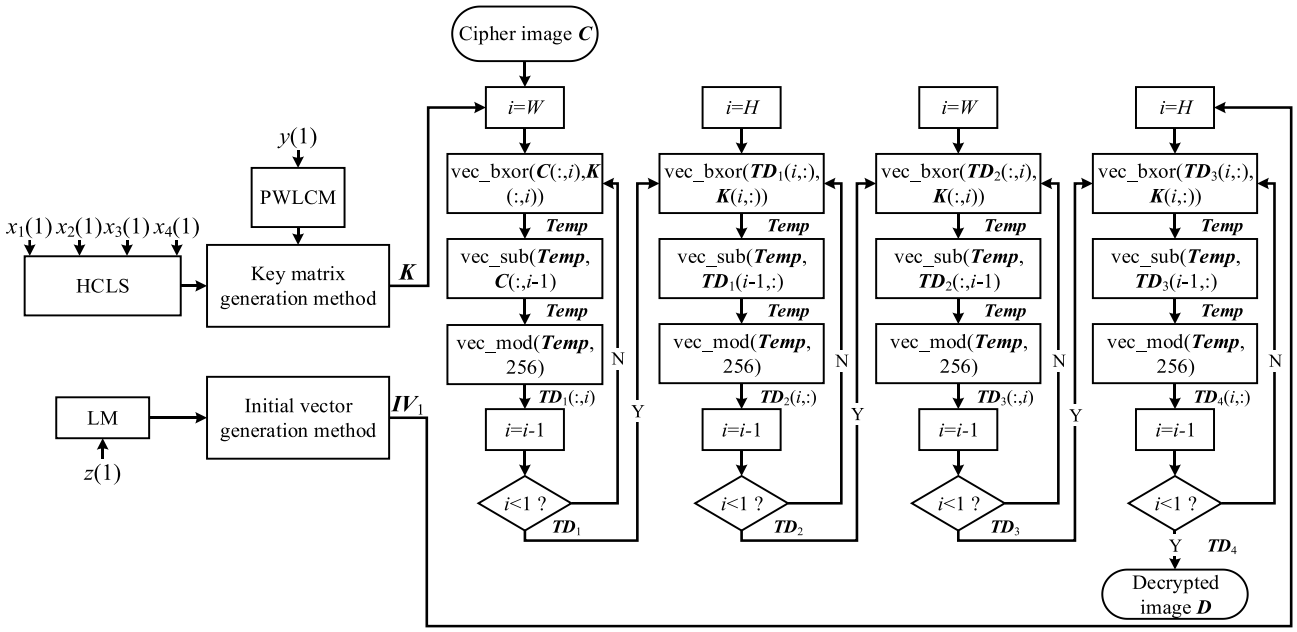

FIGURE 6. Flow diagram of decryption.

encrypt the first row. After the third round of diffusion, temporary cipher image $\boldsymbol{TC}_3$ is created, as illustrated in Fig. 5(d).

$$\begin{cases} \boldsymbol{TC}_3(0,:) = \boldsymbol{IV}_3 = \boldsymbol{TC}_2(H,:) \\ \boldsymbol{temp} = (\boldsymbol{TC}_2(i,:) + \boldsymbol{TC}_3(i-1,:)) \bmod 256 \\ \boldsymbol{TC}_3(i,:) = \text{bitxor}(\boldsymbol{K}(i,:), \boldsymbol{temp}) \\ i = 1, 2, \ldots, H-1, H \end{cases} \tag{8}$$

Step 5: Use $\boldsymbol{K}$ for column-by-column encryption of $\boldsymbol{TC}_3$ from left to right, as defined in Eq. (9), and $\boldsymbol{IV}_4 = \boldsymbol{TC}_3(:, W)$ to encrypt the first column. After the fourth round of diffusion, temporary cipher image $\boldsymbol{TC}_4$ is created, as illustrated in Fig. 5(e).

$$\begin{cases} \boldsymbol{TC}_4(:,0) = \boldsymbol{IV}_4 = \boldsymbol{TC}_3(:,W) \\ \boldsymbol{temp} = (\boldsymbol{TC}_3(:,i) + \boldsymbol{TC}_4(:,i-1)) \bmod 256 \\ \boldsymbol{TC}_4(:,i) = \text{bitxor}(\boldsymbol{K}(:,i), \boldsymbol{temp}) \\ i = 1, 2, \ldots, W-1, W \end{cases} \tag{9}$$

Step 6: Output $\boldsymbol{TC}_4$ as the final cipher image $\boldsymbol{C}$ as shown in Fig. 5(f).

D. THE DECRYPTION PROCESS

The decryption process is the converse of the encryption process, as shown in the flow diagram in Fig. 6, where function vec_sub() represents a vectorized subtraction operation.

IV. EXPERIMENTAL RESULTS AND ANALYSES

We used common tests to thoroughly evaluate the security and performance of the proposed algorithm. The algorithm and tests were implemented in MathWorks Matlab 2016b, which provides all the vectorized operations for our algorithm, running on a personal computer equipped with an Intel® Core i5-6500 processor at 3.2 GHz, 16 GB memory, and Windows 7 operating system. For the simulation, we randomly generated a session key consisting of $pre_1 = 157$, $x_1(1) = 0.737$, $x_2(1) = 0.962$, $x_3(1) = 0.175$, $x_4(1) = 0.504$ for HCLS, $pre_2 = 103$, $y(1) = 0.357$ for PWLCM, and $pre_3 = 54$, $z(1) = 0.985$ for LM. The images for testing had a resolution of 512 × 512 pixels and 8-bit grayscale level. Fig. 7 shows the simulation results of eight images (Lena, Man, Finger, Brain, Aerial, Baboon, Peppers, and Ruler) from different public image datasets.

The first column and second column of Fig. 7 show that the proposed algorithm can encrypt a meaningful image as an unordered image without leaking useful information. The third column of Fig. 7 shows that the encrypted images can be successfully recovered using the decryption algorithm and a correct session key. The simulation results demonstrate the feasibility of the proposed algorithm.

Below, we report the results of common test methods that verify the security and operational efficiency of the proposed image encryption algorithm.

A. HISTOGRAM ANALYSIS

The grayscale histogram shows the distribution of a digital image's pixels. An ideal cipher image should have a uniformly distributed histogram with all the pixels being equiprobable to hide the pixel frequency of the plaint image. Fig.8 shows the histograms of the plain and cipher images. In the second column of Fig.8, the histograms of the plain images have noticeable distribution characteristics. After applying the proposed encryption algorithm, the histograms of the corresponding cipher images are uniformly distributed, as shown in the fourth column of Fig.8.

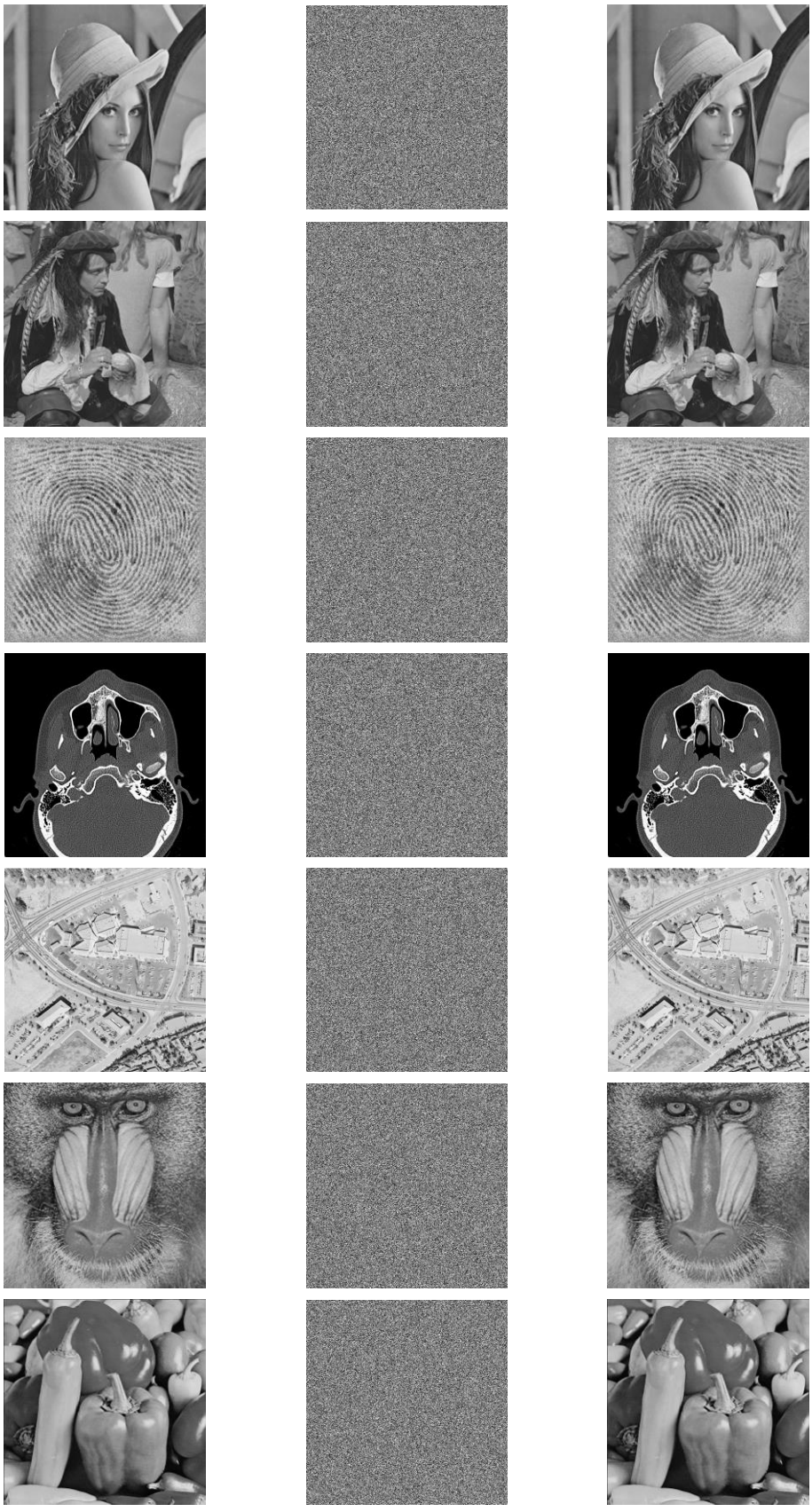

FIGURE 7. Simulation results. The plain images, cipher images, and decrypted images are respectively in the first column, second column, and third column.

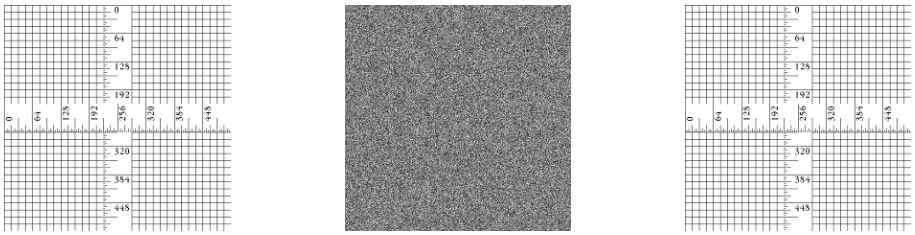

FIGURE 7. *(Continued.)* **Simulation results. The plain images, cipher images, and decrypted images are respectively in the first column, second column, and third column.**

TABLE 1. Results of chi-square test (set $\alpha = 0.05$).

Image	*P*-value	Image	*P*-value
Lena	0.95179	Aerial	0.22012
Man	0.64433	Baboon	0.90473
Finger	0.77183	Peppers	0.97097
Brain	0.49831	Ruler	0.89817

In addition, we calculate chi-square (χ^2) values of the above images by Eq. (10) to further analyze the distributions of pixels.

$$\chi^2 = \sum_{i=1}^{L} \frac{(f_i - p_i)^2}{p_i} \tag{10}$$

and the pixel level L of grayscale is 256, f_i and p_i are the observed frequency and expected frequency of each pixel value. For an ideal cipher image, the χ^2 values should be 293.24783. Then, we set the significant level $\alpha = 0.05$, and obtain the results of *P*-values as shown in Table 1. Since all the *P*-values are greater than 0.05, it indicates that any plain image encrypted by our algorithm has a good random distribution to resist frequency attacks.

B. STATISTICAL ANALYSIS

In this subsection, we use the NIST SP 800-22 test suit, which consists of 15 statistical tools to check the randomness of a sequence, to verify the statistical performance of the proposed algorithm. Both the key matrix used in the encryption and final cipher images are converted to binary sequences for the test. And the significant level α is set to 0.01, which means the result of each test must be greater than 0.01 to consider a sequence to be random with a confidence of 99%. In Table 2, it can be observed that all the *P*-values exceed the threshold of randomness statistical tests. Hence, we can conclude that the proposed image encryption algorithm has strong robustness against statistical attacks.

C. KEY SPACE ANALYSIS

Owing to the rapid development of computing devices, exhaustive attacks threaten symmetric encryption algorithms. The key space of a secure encryption algorithm must be larger than 2^{128} to resist brute-force attacks [38], [39]. In our algorithm, the session key has two parts: 1) pre-iterations of the chaotic systems with 16-bit unsigned integers, and 2) initial values of the chaotic systems with double-precision floating-point numbers. Thus, the key space of the proposed algorithm is $(2^{16})^3 \times (10^{15})^6 \approx 2^{345}$. Table 3 lists the comparison of key spaces between various image encryption algorithms. Although a larger key space provides higher resistance against brute-force attacks, it also means harder transmission. Since NIST declares the key space more than 256 is enough for most encryption scenarios [12], our algorithm can achieve the same protective effect against brute force attacks as some algorithms with larger key space.

D. PLAINTEXT SENSITIVITY ANALYSIS

To resist a differential attack, a secure encryption algorithm must be sensitive to minor changes in the plain image. In other words, even one bit change in any position of a plain image should make the encryption generate a totally different cipher image. There are two common standards given by Eq. (11), NPCR (number of pixel change rate), and UACI (unified average changing intensity), to measure the sensitivity to one bit change in plain images.

$$\begin{cases} \mathrm{NPCR} = \dfrac{\sum_{i=1}^{W}\sum_{j=1}^{H} D(i,j)}{W \times H} \times 100\% \\ \mathrm{UACI} = \dfrac{1}{255 \times W \times H} \\ \times \left[\sum_{i=1}^{W}\sum_{j=1}^{H} C_1(i,j) - C_2(i,j) \right] \times 100\% \\ D(i,j) = \begin{cases} 0, & \text{if } C_1(i,j) = C_2(i,j) \\ 1, & \text{if } C_1(i,j) \neq C_2(i,j) \end{cases} \end{cases} \tag{11}$$

where $\boldsymbol{C}_1$ and $\boldsymbol{C}_2$ are cipher images.

We evaluated the ability of the proposed encryption algorithm to resist a differential attack as follows. First, we changed one bit of a randomly selected pixel in the original plain image. Then, we used the same session key to encrypt both the original and modified plain images. Thus, we obtained two cipher images, $\boldsymbol{C}_1$ and $\boldsymbol{C}_2$. Finally, we used Eq. (11) to calculate NPCR and UACI between $\boldsymbol{C}_1$ and $\boldsymbol{C}_2$. We evaluated all the test images 100 times and obtained the average NPCR and UACI listed in Table 4. Our algorithm can effectively resist a differential attack because the

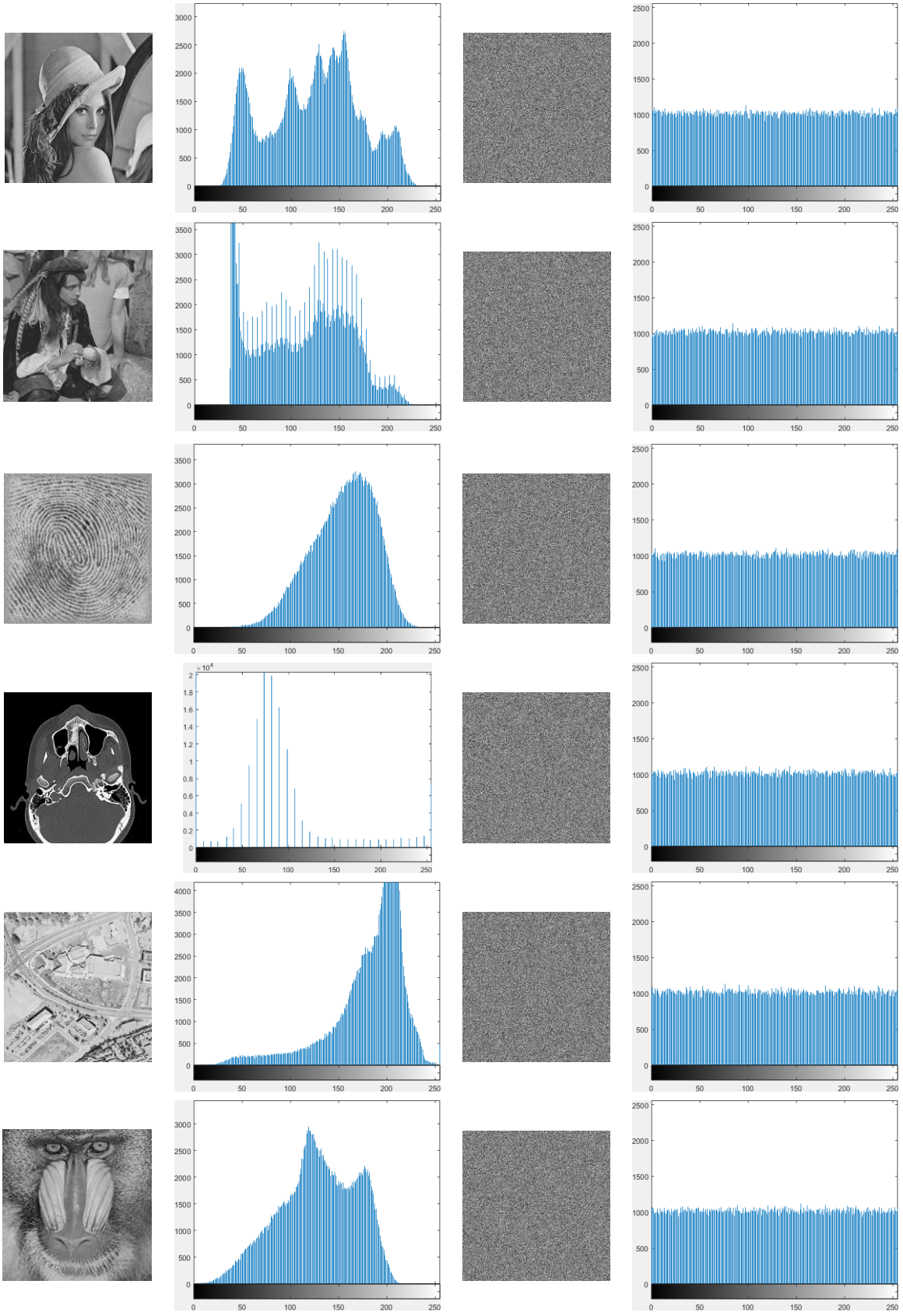

FIGURE 8. Histograms of plain images (presented in the first column) in the second column, and cipher images (presented in the third column) in the fourth column.

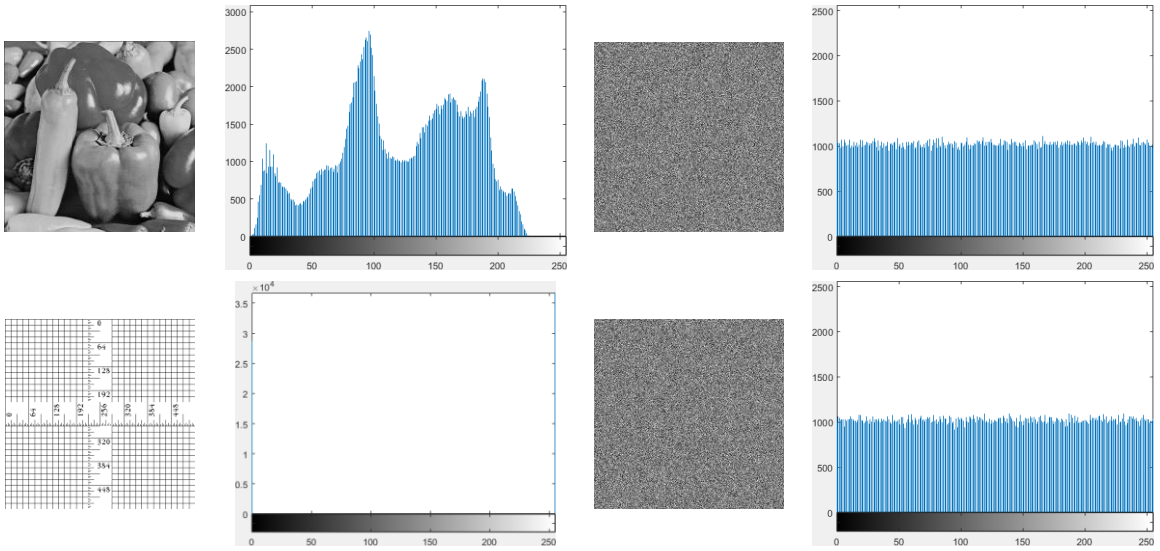

FIGURE 8. *(Continued.)* **Histograms of plain images (presented in the first column) in the second column, and cipher images (presented in the third column) in the fourth column.**

TABLE 2. ***P*-values of the NIST SP 800-22 test suit (set $\alpha = 0.01$).**

Test	*P*-value								
	K	Lena	Man	Finger	Brain	Aerial	Baboon	Peppers	Ruler
Frequency	0.9711	0.7029	0.2376	0.9815	0.4187	0.6915	0.6843	0.3118	0.2695
Block Frequency	0.1942	0.9831	0.6823	0.2127	0.4089	0.5349	0.2138	0.8799	0.2592
Cumulative Sums	0.7145	0.1201	0.1138	0.8219	0.9864	0.2204	0.3271	0.1355	0.4969
Runs	0.5754	0.6712	0.7373	0.7622	0.7192	0.1688	0.4896	0.8145	0.3382
Longest Runs of Ones	0.1344	0.1895	0.9812	0.4638	0.7093	0.7847	0.2893	0.1865	0.6362
Rank	0.4729	0.8548	0.7324	0.8699	0.3173	0.3178	0.3118	0.5477	0.3916
Spectral DFT	0.1477	0.9313	0.9402	0.2989	0.7023	0.6531	0.2059	0.7909	0.2916
Nonperiodic Template Matchings	0.6649	0.1432	0.9079	0.1461	0.7089	0.4839	0.2718	0.7892	0.5851
Overlapping Template Matchings	0.2683	0.5123	0.7959	0.2943	0.5043	0.4383	0.2465	0.205	0.5973
Universal Statistical	0.7701	0.8001	0.7724	0.9001	0.9015	0.2389	0.8269	0.9812	0.1802
Approximate Entropy	0.3159	0.5933	0.2189	0.9082	0.3694	0.8861	0.4809	0.8713	0.8352
Random Excursions	0.9753	0.0773	0.8636	0.7862	0.5803	0.3869	0.2617	0.7301	0.2606
Random Excursions Variant	0.6124	0.7555	0.3385	0.4897	0.4432	0.2465	0.7755	0.4274	0.1541
Serial	0.5465	0.3276	0.3721	0.5498	0.7791	0.1867	0.8719	0.3479	0.1711
Linear Complexity	0.4811	0.6048	0.5412	0.4927	0.2917	0.7556	0.7015	0.5102	0.9563
Result	Pass	Pass	Pass	Pass	Pass	Pass	Pass	Pass	Pass

TABLE 3. **Key space of various image encryption algorithms.**

Algorithm	Ours	Ref. [38]	Ref. [39]	Ref. [40]	Ref. [41]	Ref. [42]	Ref. [43]	Ref. [44]	Ref. [45]
Key space	2^{345}	2^{297}	2^{399}	2^{216}	2^{256}	2^{465}	2^{212}	2^{512}	2^{418}

experimental results are close to the expected values: $\text{NPCR}_\text{E} = 99.6094\%$ and $\text{UACI}_\text{E} = 33.4636\%$ [1], [2]. Furthermore, the results of the other algorithms indicate the superior performance of the proposed algorithm. Thus, the proposed encryption algorithm can provide higher security for image communication under strong differential attacks.

E. KEY SENSITIVITY ANALYSIS

A secure encryption algorithm must also be sensitive to minor changes in the session key. In other words, even one bit change in the session key should make the same plain image to be encrypted in a different cipher image. We divided the key sensitivity test into two stages: encryption and decryption.

TABLE 4. Average NPCR and UACI obtained from the plaintext image sensitivity test (%).

Image	Standard	Ours	Ref [38]	Ref [39]	Ref [40]	Ref [41]	Ref. [42]	Ref. [43]	Ref. [44]	Ref. [45]
Lena	NPCR	99.6091	99.6122	99.6093	99.6114	99.6106	99.81	99.61	99.6185	99.63
	UACI	33.4709	33.4573	33.5989	33.4523	33.4669	33.40	33.43	33.4561	28.5142
Man	NPCR	99.6112	99.6092	-	99.6089	99.6081	-	99.61	99.6078	-
	UACI	33.4638	33.4682	-	33.4713	33.4662	-	33.44	33.4821	-
Finger	NPCR	99.6083	99.6118	-	-	-	-	-	99.6017	-
	UACI	33.4705	33.4691	-	-	-	-	-	33.4162	-
Brain	NPCR	99.6125	-	-	-	-	-	-	99.6185	-
	UACI	33.4655	-	-	-	-	-	-	33.4550	-
Aerial	NPCR	99.6089	-	-	99.6043	99.6091	-	99.61	99.6063	-
	UACI	66.4643	-	-	33.2875	33.4826	-	33.46	33.4969	-
Baboon	NPCR	99.6105	99.6108	99.6091	99.6016	99.6097	-	99.61	99.6109	99.63
	UACI	33.4661	33.4653	33.5381	33.4039	33.4660	-	33.48	33.5034	27.0424
Peppers	NPCR	99.6078	99.6102	99.6202	99.6115	-	-	99.61	99.6044	99.62
	UACI	33.4637	33.4691	33.6602	33.4245	-	-	33.47	33.4117	29.4536
Ruler	NPCR	99.6096	-	-	-	-	-	99.61	99.6239	-
	UACI	33.4635	-	-	-	-	-	33.52	33.4920	-

TABLE 5. Average NPCR and UACI obtained from the encryption key sensitivity test (%).

Value name	Original value	Modified value	NPCR			UACI		
			Lena	Peppers	Baboon	Lena	Peppers	Baboon
pre_1	157	158	99.6048	99.6158	99.6008	33.4550	33.4742	33.4599
$x_1(1)$	0.737	$0.737+10^{-15}$	99.6156	99.6032	99.6011	33.4628	33.4588	33.4569
$x_2(1)$	0.962	$0.962+10^{-15}$	99.6096	99.6115	99.6066	33.4674	33.4596	33.4738
$x_3(1)$	0.175	$0.175+10^{-15}$	99.6149	99.6123	99.6014	33.4568	33.4736	33.4508
$x_4(1)$	0.504	$0.504+10^{-15}$	99.6022	99.6124	99.6011	33.4704	33.4749	33.4752
pre_2	103	104	99.6069	99.6128	99.6037	33.4763	33.4577	33.4789
$y(1)$	0.357	$0.357+10^{-15}$	99.6037	99.6080	99.6016	33.4596	33.4583	33.4776
pre_3	54	55	99.6055	99.6086	99.6037	33.4534	33.4761	33.4776
$z(1)$	0.985	$0.985+10^{-15}$	99.6164	99.6166	99.6131	33.4728	33.4620	33.4694

In the first stage, we slightly modified the seven values of the session key. In each round of the test, we slightly changed the least significant digit of the value. Then, we encrypted the test image using the original and modified session keys. Finally, we obtained NPCR and UACI to compare the two cipher images. Table 5 lists the results of this stage. The values of pre_1, pre_2, and pre_3 were only increased by 1, while those of $x_1(1)$, $x_2(1)$, $x_3(1)$, $x_4(1)$, $y(1)$, and $z(1)$ were only increased by 10^{-15}. The NPCR and UACI values indicate that each pair of cipher images encrypted using slightly different session keys are highly dissimilar. Thus, the proposed image encryption algorithm is sensitive to the encryption key.

In the second stage, we used the abovementioned session keys to evaluate the decryption key sensitivity of the proposed algorithm. Unlike the previous test, we used the original and modified session keys to decrypt the same cipher image, and then we obtained a correctly decrypted image and an incorrectly decrypted image, as illustrated for the Lena image in Fig. 9. Fig. 9(a) and (b) show that even by only adding 10^{-15} to x_1, the cipher image fails to be correctly decrypted and results in salt-and-pepper noise. Only using the exact decryption key allows the cipher image to be recovered as the original plain image, as shown in Fig. 9(c) and (d).

The NPCR and UACI values between pairs of incorrectly decrypted images and plain images are listed in Table 6. Any minor change in the decryption key leads to failed decryption. Thus, the proposed decryption algorithm has high key sensitivity and can resist brute-force attacks.

F. ANALYSIS OF THE CORRELATION BETWEEN ADJACENT PIXELS

A high correlation between adjacent pixels hinders the effective hiding of plain image information. Hence, a secure encryption algorithm should minimize the correlation between adjacent pixels, with a low correlation between adjacent pixels in cipher images indicating the high security of an encryption algorithm.

For the pixel correlation test, we randomly selected 10,000 pairs of adjacent pixels along with the horizontal, vertical, and diagonal directions from the plain image of

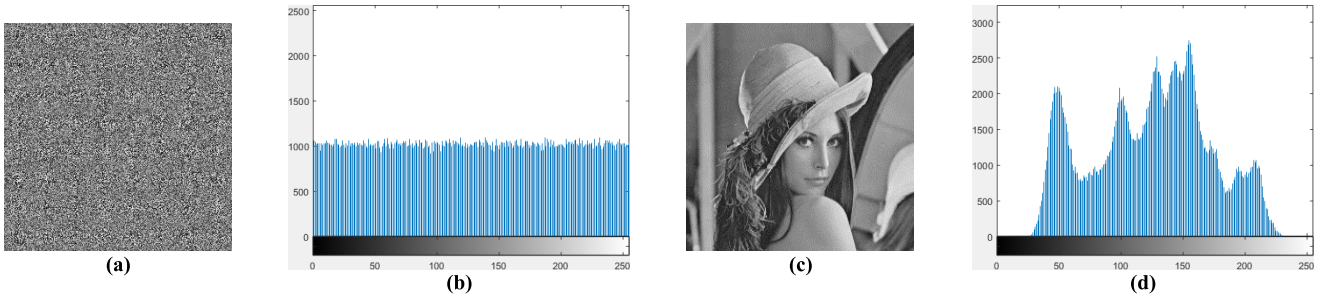

FIGURE 9. Decryption key sensitivity test on Lena image. (a) Decrypted image using $x_1 + 10^{-15}$ and (b) its histogram. (c) Decrypted image using the correct session key and (d) its histogram.

TABLE 6. Average NPCR and UACI obtained from the decryption key sensitivity test (%).

Value name	Original value	Modified value	NPCR			UACI		
			Lena	Peppers	Baboon	Lena	Peppers	Baboon
pre_1	157	158	99.6058	99.6009	99.6153	33.4554	33.4526	33.4518
$x_1(1)$	0.737	0.737+10^{-15}	99.6025	99.6261	99.5975	33.4732	33.4709	33.4619
$x_2(1)$	0.962	0.962+10^{-15}	99.6088	99.6174	99.6270	33.4714	33.4588	33.4592
$x_3(1)$	0.175	0.175+10^{-15}	99.6093	99.6074	99.6038	33.4615	33.4654	33.4617
$x_4(1)$	0.504	0.504+10^{-15}	99.6086	99.6152	99.6059	33.4501	33.4653	33.4550
pre_2	103	104	99.6161	99.6202	99.5936	33.4583	33.4737	33.4521
$y(1)$	0.357	0.357+10^{-15}	99.6091	99.6142	99.6245	33.4741	33.4701	33.4677
pre_3	54	55	99.5943	99.6252	99.6232	33.4665	33.4656	33.4693
$z(1)$	0.985	0.985+10^{-15}	99.5909	99.5989	99.6141	33.4592	33.4699	33.4709

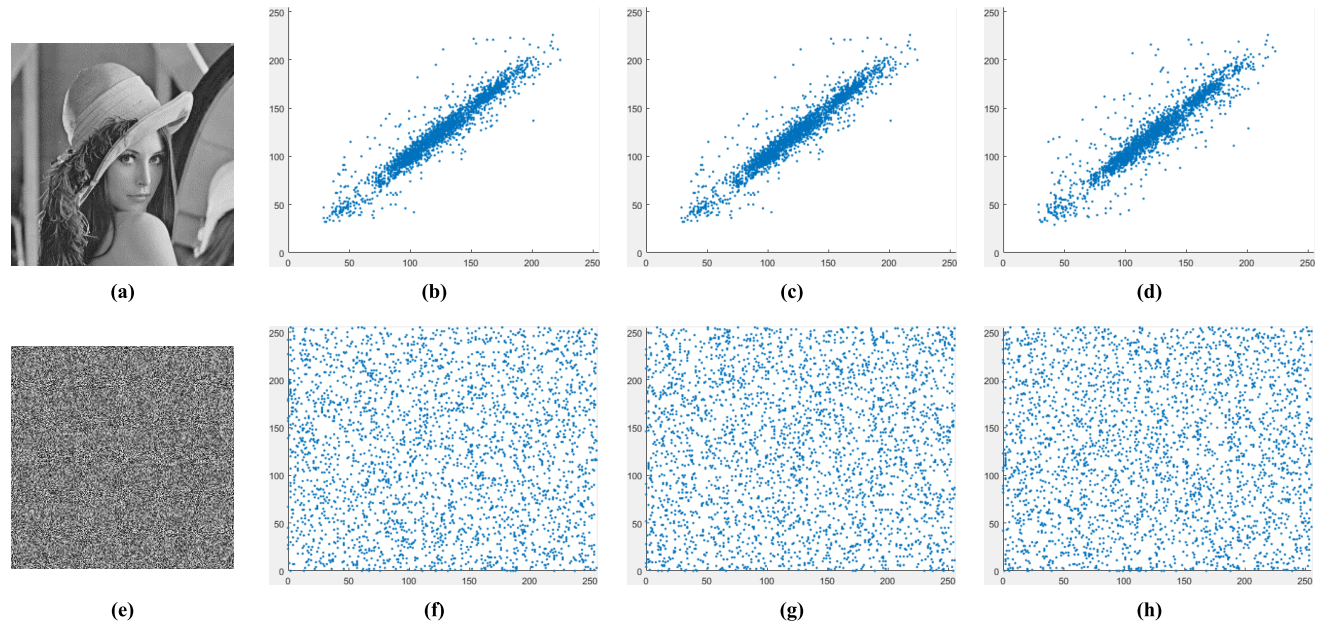

FIGURE 10. Correlation between adjacent pixels of (a) Lean along (b) horizontal, (c) vertical, and (d) diagonal directions. Correlation between adjacent pixels of (e) cipher image along (f) horizontal, (g) vertical, and (h) diagonal directions.

Lena and its corresponding cipher image. Fig. 10 shows the correlation distribution. In Fig. 10(b)–(d), the distributions of adjacent pixels on the plain images are highly concentrated. In contrast, the distributions of adjacent pixels in the cipher images are randomly distributed, as shown in Fig. 10(f)–(h). Therefore, the proposed encryption algorithm can substantially reduce the correlation between adjacent pixels for increased security.

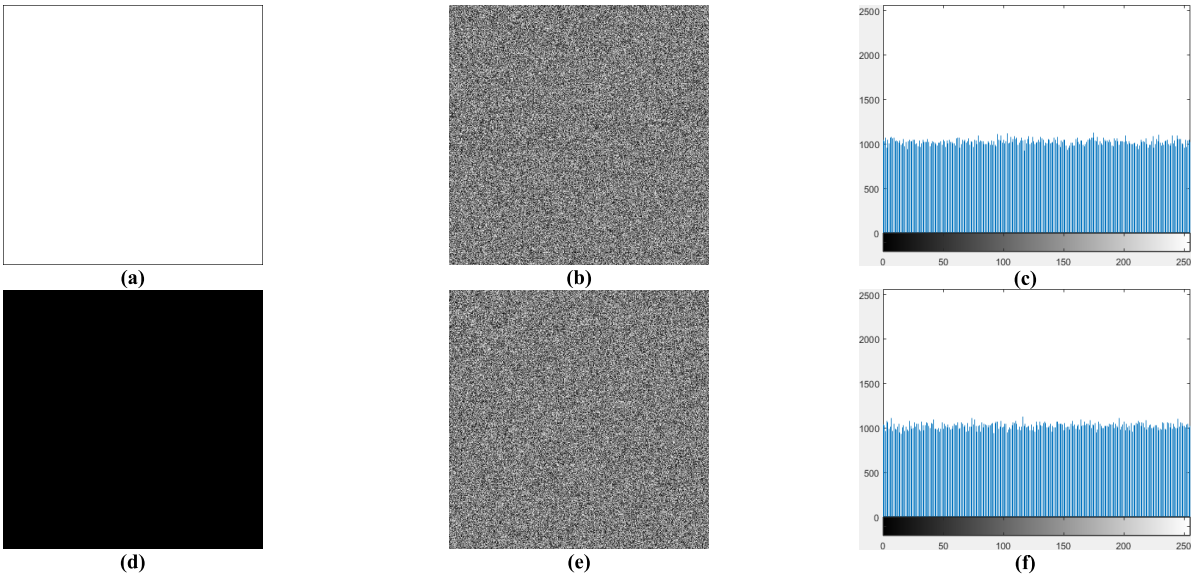

FIGURE 11. Evaluation of all-black and all-white image encryption. (a) All-white image and its (b) cipher image. (c) Histogram of all-white cipher image. (d) All-black image and its (e) cipher image. (f) Histogram of all-black cipher image.

TABLE 7. Results of correlation coefficients between adjacent pixels.

Image		Direction		
		Horizontal	Vertical	Diagonal
Lena	Plain	0.9841	0.9691	0.91639
	Cipher	-0.0002	-0.0007	-0.0016
Man	Plain	0.9675	0.9593	0.9432
	Cipher	-0.0015	0.0024	0.0004
Finger	Plain	0.9037	0.8869	0.8119
	Cipher	-0.0013	-0.0001	-0.0007
Brain	Plain	0.9583	0.9467	0.9185
	Cipher	0.0009	0.0001	-0.0008
Aerial	Plain	0.8549	0.8993	0.8003
	Cipher	-0.0006	-0.0005	-0.0007
Baboon	Plain	0.9100	0.9322	0.8647
	Cipher	0.0001	-0.0003	0.0011
Peppers	Plain	0.9764	0.9733	0.9651
	Cipher	-0.0009	0.0017	-0.0001
Ruler	Plain	0.4599	0.4494	-0.0291
	Cipher	0.0003	-0.0004	-0.0008

We further used correlation coefficient r_{xy} to measure the robustness of the proposed image encryption algorithm against statistical attacks given by

$$\begin{cases} \bar{x} = \dfrac{1}{N}\sum_{i=1}^{N} x_i, \quad \bar{y} = \dfrac{1}{N}\sum_{i=1}^{N} y_i \\ r_{xy} = \dfrac{\sum_{i=1}^{N}(x_i - \bar{x})(y_i - \bar{y})}{\sqrt{\left(\sum_{i=1}^{N}(x_i - \bar{x})^2\right)\left(\sum_{i=1}^{N}(y_i - \bar{y})^2\right)}} \end{cases} \tag{12}$$

TABLE 8. Correlation coefficients of lena using various algorithms.

Algorithm	Direction		
	Horizontal	Vertical	Diagonal
Ours	-0.0002	-0.0007	-0.0016
Ref. [38]	-0.0052	0.0031	-0.0003
Ref. [39]	0.0052	0.0052	0.0052
Ref. [40]	-0.0381	-0.0291	0.0027
Ref. [41]	0.0052	-0.0001	-0.0022
Ref. [42]	-0.0019	0.0105	-0.0019
Ref. [43]	0.0010	-0.0026	0.0017
Ref. [44]	0.0015	-0.0090	-0.0120
Ref. [45]	0.0055	-0.0053	-0.0100

where $N = 10{,}000$ and x_i and y_i $(i = 1, 2, \ldots, N)$ are pairs of adjacent pixels randomly selected from the image. Table 7 lists the correlation coefficient between adjacent pixel pairs on test images. The value of r_{xy} in all the plain images is close to one along each direction, and that in all the cipher images is close to zero along each direction.

Comparison results of the correlation coefficient on the Lena image are listed in Table 8. The proposed encryption algorithm provides a low correlation between adjacent pixels.

Overall, the proposed algorithm provides satisfactory encryption for high resistance to correlation attacks.

G. INFORMATION ENTROPY ANALYSIS

Information entropy is an important measure of randomness on an image. A higher entropy indicates more information and more randomness, and the entropy reaches its maximum only if the probabilities of all the information elements

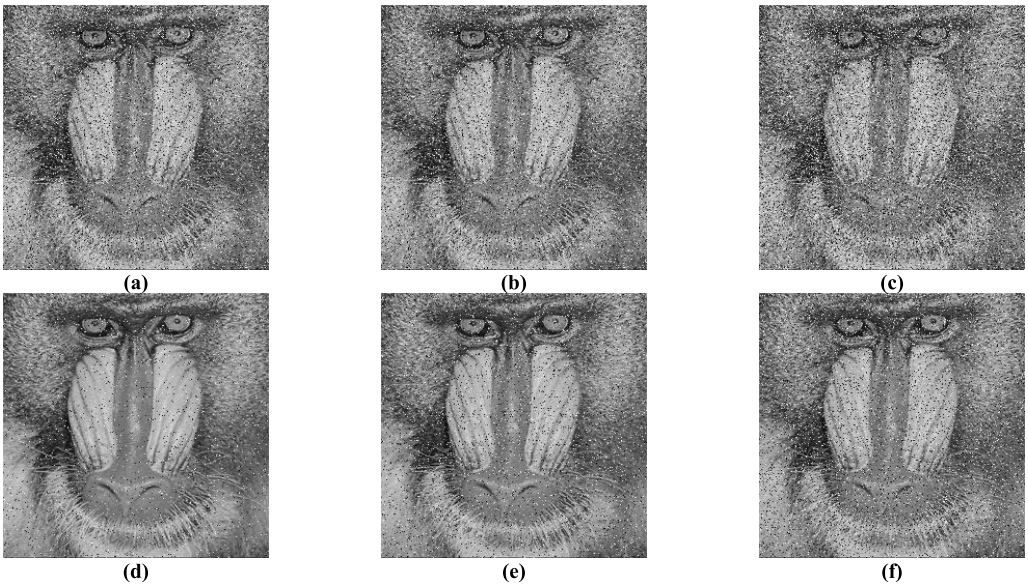

FIGURE 12. Decrypted images from cipher images polluted by Gaussian white noise with zero mean and variances of (a) 0.001, (b) 0.003, and (c) 0.005 and by (d) 1%, (e) 3%, and (f) 5% salt-and-pepper noise.

TABLE 9. Information entropy of cipher images obtained using various encryption algorithms.

Image	Plaintext	Ours	Ref. [38]	Ref. [39]	Ref. [40]	Ref. [41]	Ref. [42]	Ref. [43]	Ref. [44]	Ref. [45]
Lena	7.4451	7.9996	7.9973	7.9992	7.9972	7.9977	7.9987	7.9971	7.9939	7.9881
Man	7.2367	7.9998	7.9998	-	7.9998	7.9998	-	-	-	7.9890
Finger	7.0153	7.9995	7.9975	-	-	-	-	-	-	-
Brain	3.1047	7.9996	-	-	-	-	-	7.9967	-	-
Aerial	6.9939	7.9997	-	-	7.9998	-	-	7.9972	7.9972	-
Baboon	7.2925	7.9999	7.9998	7.9993	7.9998	7.9998	-	7.9970	-	7.9866
Peppers	7.5937	7.9996	7.9993	7.9970	7.9992	7.9992	7.9979	7.9972	7.9973	7.9894
Ruler	0.5000	7.9996	-	-	-	-	-	7.9974	-	-

TABLE 10. Experimental results for all-black and all-white images.

Test		χ^2 test	NPCR(%)		UACI(%)		Entropy	Correlation coefficient		
			Min	Max	Min	Max		Horizontal	Vertical	Diagonal
All-blace	Ours	0.2342	99.6018	99.6227	33.4559	33.4644	7.9991	0.0014	-0.0007	0.0033
	Ref. [40]	-	99.6328		33.4965		7.9975	0.0095	-0.0249	0.0027
	Ref. [44]	Pass	99.6143		33.4719		7.9976	-0.0049	0.0067	-0.0006
All-white	Ours	0.3508	99.5993	99.6244	33.4528	33.4684	7.9994	-0.0038	0.0016	0.0028
	Ref. [40]	-	99.6129		33.5079		7.9974	0.0313	0.0214	0.0083
	Ref. [44]	Pass	99.6075		33.4302		7..9973	0.0033	-0.0051	0.0093

are equal. The information entropy is defined as

$$\begin{cases} \sum_{i=0}^{L} p(g_i) = 1 \\ H(g) = -\sum_{i=0}^{L} p(g_i) \log_2 p(g_i) \end{cases} \tag{13}$$

where L denotes the number of possible elements g_i and $p(g_i)$ represents the frequency of element g_i, with the entropy of an ideal random 8-bit grayscale image being 8. Table 9 lists the information entropy values for various encryption algorithms. The information entropy of the cipher images is close to eight, indicating that the proposed algorithm can resist entropy attacks. Compared with existing algorithms, our proposal has made some progress regarding information entropy.

H. CHOSEN-PLAINTEXT ATTACK ANALYSIS

A secure encryption algorithm must resist chosen-plaintext attacks by preventing an attacker from distinguishing two encryptions even if the attacker can elaborately choose the

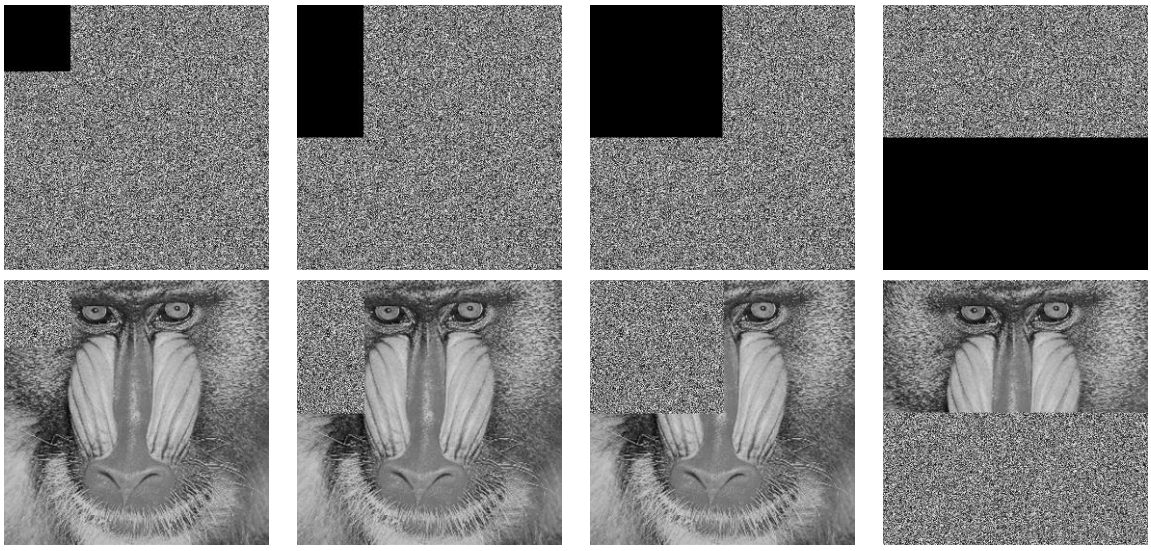

FIGURE 13. Data loss decryption results. (a) 1/16 cropping image and its decrypted image, (b) 1/8 cropping image and its decrypted image, (c) 1/4 cropping image and its decrypted image, and (d) 1/2 cropping image and its decrypted image.

TABLE 11. PSNR results of decrypted images.

Algorithm	Cipher image polluted by									
	salt&peppers with intensity of			Gaussian with variance of			Data loss of			
	1%	3%	5%	0.001	0.003	0.005	1/16	1/8	1/4	1/2
Ours	20.46	16.01	14.09	15.29	13.29	12.73	21.54	18.21	15.37	12.73
Ref. [44]	30.5914	19.34	10.53	14.07	9.93	9.41	-	18.20	15.22	12.23

corresponding plain images. An all-black or all-white image is often used to analyze the vulnerability of encryption algorithms [1], [2], [40], [44]. The proposed algorithm uses four-round vectorized diffusion to ensure that any pixel information spreads to the entire cipher image, thus having a high sensitivity to any plain image. Fig. 11 shows the histogram of all-black and all-white images of 512 × 512 pixels, and Table 10 lists the experimental measures. In Fig. 11, the pixel distributions of the all-black and all-white images are uniform after encryption. Thus, an attacker cannot obtain useful information from the cipher images to break the encryption algorithm. More importantly, the plaintext sensitivity, entropy, and correlation results listed in Table 8 indicate that the proposed algorithm provides an excellent performance regarding the corresponding measures, even when using these specific plain images. Therefore, the proposed image encryption algorithm can resist chosen-plaintext attacks.

I. ROBUSTNESS ANALYSIS

Noise jamming and data loss may occur when a digital image is transmitted through an unstable public channel. Suitable image encryption should be robust to noise and data loss by being able to decrypt a noisy cipher image into a recognizable plain image. Fig. 12 shows the results of noise attacks applied to the proposed image encryption algorithm.

TABLE 12. Execution time of various image encryption algorithms (unit: s).

Algorithm		Image Size		
		256×256	512×512	1024×1024
Ours	Worst	0.018	0.031	0.077
	Best	0.011	0.023	0.061
	Average	0.015	0.027	0.068
	Throughput	1.3Mbps	9.5Mbps	14.7Mbps
Ref. [38]		1.217	4.893	19.891
Ref. [39]		25kbps in normal and 210kbps in parallel		
Ref. [41]		0.053	0.158	0.806
Ref. [43]		0.133	-	-
Ref. [44]		0.380	1.431	5.719

The cipher image can be decrypted even when it is polluted by different types and intensities of noise, and the recovered Baboon image is recognizable. Fig. 13 shows the decrypted results of the cipher image with data lost 1/16, 1/8, 1/4, and 1/2. Although the cipher image can be decrypted to a meaningful image, we observe that the noise mainly concentrates somewhere. It means in some special situations, such as satellite image encryption and medical image encryption, the receiver has a certain probability of missing some key information. Alternatively, a solution to this problem is adding a scrambling process before or after the diffusion

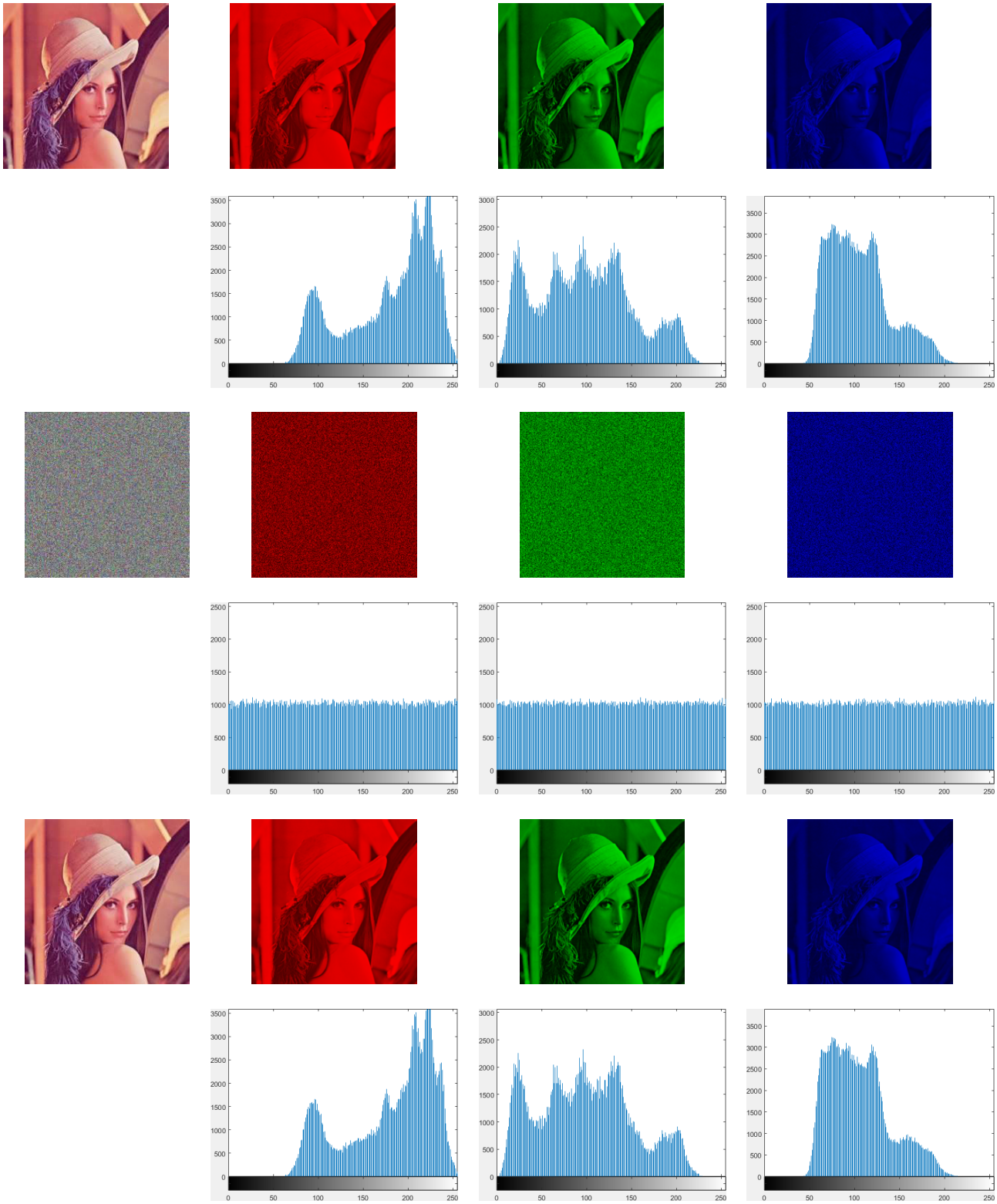

FIGURE 14. Simulation and histogram results of Lena color image. The first row shows the Lena color image and its R, G, B channels. The second row shows the distribution of pixels of Lena color image in R, G, B channels. The third row shows the cipher image and its R, G, B channels. The fourth row shows the distribution of pixels of cipher image in R, G, B channels. The fifth row shows the decrypted image and its R, G, B channels. The sixth row shows the distribution of pixels of the decrypted image and its R, G, B channels.

TABLE 13. The results of security and encryption speed tests.

	Test	γ_{xy}			χ^2	NPCR	UACI	Information entropy
		Horizontal	Vertical	Diagonal				
R	Ours	-0.0016	-0.0003	-0.0012	0.3409	99.6099%	33.4605%	7.9992
	Ref. [44]		-		Pass	99.6197%	33.4423%	7.9993
G	Ours	-0.0005	0.0011	0.0028	0.9911	99.6188%	33.4599%	7.9994
	Ref. [44]		-		Pass	99.6117%	33.4539%	7.9994
B	Ours	-0.0017	-0.0024	-0.0004	0.9392	99.6085%	33.4621%	7.9993
	Ref. [44]		-		Pass	99.6113%	33.4647%	7.9992

process, but the time consumption may cost even more than the diffusion process [43]. Therefore, our algorithm can recover a useful image from data loss in most real-time communication scenarios.

Furthermore, decrypted images with pollution and data loss are evaluated by the PSNR (Peak Signal to Noise Ratio).

$$\mathrm{PSNR} = 10\lg \frac{255 \times 255}{(1/W \times H)\sum_{i=1}^{W}\sum_{j=1}^{H}(P(i,j) - D(i,j))^2} \quad (14)$$

In Table 11, the PSNRs of images decrypted from cipher images with different pollution and data loss are presented. By comparison with previous works, our algorithm still has good performance despite the above-mentioned weakness. It indicates that the proposed image encryption algorithm has strong robustness to protect data transmission on the Internet.

J. COMPUTATIONAL COST ANALYSIS

Security and execution speed are the most important measures of the applicability of an encryption algorithm. The abovementioned experimental results verify the high security of the proposed algorithm. Here, we analyze the execution time. The proposed image encryption algorithm consists of three main parts: key matrix generation, initial vector generation, and vectorized diffusion process. For key matrix generation, the time complexities of the HCLS iteration, PWLCM iteration, and matrix generation are $\boldsymbol{O}(2W)$, $\boldsymbol{O}(2H)$, and $\boldsymbol{O}(H)$, respectively. For initial vector generation, the time complexity is $\boldsymbol{O}(W)$, and for vectorized diffusion process, the time complexity is $\boldsymbol{O}(2W + 2H)$. Therefore, the total time complexity of the proposed algorithm is $\boldsymbol{O}(5W + 5H)$. For large W and H, the time complexity can be approximated as $\boldsymbol{O}(W+H)$. Although some algorithms [38], [41] optimize the time complexity of the diffusion process to the order of $\boldsymbol{O}(W + H)$, their time complexity for key generation is still in the order of $\boldsymbol{O}(WH)$. Hence, the proposed algorithm can provide a faster execution.

For the programming environment considered in this study, the execution time of the proposed algorithm on test images from the USC-SIPI Image Database [55] is listed in Table 12. Although MATLAB has low efficiency, the proposed encryption algorithm is still fast. The improvements in key generation and diffusion process substantially increase the running speed of the proposed algorithm compared with existing algorithms even when considering programming environment differences. Hence, the proposed encryption algorithm can guarantee image real-time transmission as well as image security.

V. PERFORMANCE ANALYSIS OF COLOR IMAGES

In this section, the proposed algorithm is evaluated by security tested on color images.

A. SIMULATION AND HISTOGRAM RESULTS

The color image consists of pixels in the R channel, G channel, and B channel. Since it is more expressive than the grayscale image, it has more extensive application prosperity. The simulation and histogram results of the Lean color image are shown in Fig. 14. The encryption and decryption results are respectively shown in the third row and fifth row of Fig. 14 And by comparison with the second row and fourth row of Fig. 14, we can conclude that the distributions of pixels in all channels have been hidden after being encrypted by the proposed algorithm. Hence, the results indicate that our algorithm is also suitable to deal with color images.

B. OTHER ANALYSES

In this part, we utilize γ_{xy}, χ^2, NPCR, UACI, and information entropy tests to evaluate the security performance of our algorithm on color images, and obtain the time consumption of color image encryption (execution time and throughput are 0.063s and 12.6 Mbps). Table 13 shows the results of all the tests, and also demonstrates the comparisons with the results of other algorithms. Since the results are all close to ideal values and are superior to the previous algorithms, we can safely conclude that the proposed image encryption algorithm also has good security and speed performance for color images, not just for grayscale images.

VI. CONCLUSION

We proposed a secure and fast image encryption algorithm using hyper-chaos based key generator and vector operation. Aiming to reduce the time consumption of key stream generation, we present a novel method to post-process key stream generated from the general method. As a result, the HCLS only iterates $2W$ times rather than $W \times H$ times to create

a key matrix with the same size as the plain image (W and H are the width and height of the plain image respectively). During the key matrix generation process, a PWLCM is employed as a random selector to control the bitwise XOR operation between the quantified hyperchaotic sequences, which can further enhance the randomness and unpredictability of the key matrix. Then, considering two-dimensional images, we introduce the vector operation into the CBC based diffusion process, so the plain image can be implicit parallel encrypted row by row and column by column with high efficiency. Furthermore, by using an initial vector as a chain between two diffusion rounds, any pixel information and key information can be diffused to the whole cipher image. Thus, even a minor change of the session key or the plain image completely changes the resulting cipher image. In addition, we apply an LM to fast generate an initial vector for the first diffusion round, which can facilitate the storage and transmission of the initial vector. Experimental results show that the proposed encryption algorithm has a large key space of 2^{345}, high plaintext sensitivity with NPCR near 99.6094 and UACI near 33.4636, and high session key sensitivity to resist statistical, brute-force, differential, and some other common attacks. Besides, it achieves high performance regarding information entropy >7.999, and noise and data loss robustness with PSNR $>$ 10db. Moreover, tests on all-black and all-white images verify the chosen-plaintext attack resistance of our algorithm. In addition, the positive results of tests on color images indicate that our algorithm has a wide application perspective. Finally, the time complexity of our algorithm is in the order of $\boldsymbol{O}(W+H)$, which supports the algorithm to encrypt a 512 $\times$ 512 image in 0.03s. Overall, despite some respects, such as key space and data loss resistance, show slightly insufficiently, the proposed image encryption algorithm still meets the security, efficiency, and robustness requirements for most daily image confidential communications.

REFERENCES

[1] M. Khan and T. Shah, "A literature review on image encryption techniques," *3D Res.*, vol. 5, no. 4, pp. 5–29, Dec. 2014.

[2] M. Kaur and V. Kumar, "A comprehensive review on image encryption techniques," *Arch. Comput. Methods Eng.*, vol. 27, no. 1, pp. 15–43, Jan. 2020.

[3] D. Xiao, X. Liao, and P. Wei, "Analysis and improvement of a chaos-based image encryption algorithm," *Chaos, Solitons Fractals*, vol. 40, no. 5, pp. 2191–2199, 2009.

[4] M. Kaur, D. Singh, and R. S. Uppal, "Parallel strength Pareto evolutionary algorithm-II based image encryption," *IET Image Process.*, vol. 14, no. 6, pp. 1015–1026, May 2020.

[5] H. M. Ghadirli, A. Nodehi, and R. Enayatifar, "An overview of encryption algorithms in color images," *Signal Process.*, vol. 164, pp. 163–185, Nov. 2019.

[6] N. Rawat, B. Kim, I. Muniraj, G. Situ, and B.-G. Lee, "Compressive sensing based robust multispectral double-image encryption," *Appl. Opt.*, vol. 54, no. 7, pp. 1782–1793, 2015.

[7] E. E. García-Guerrero, E. Inzunza-González, O. R. López-Bonilla, J. R. Cárdenas-Valdez, and E. Tlelo-Cuautle, "Randomness improvement of chaotic maps for image encryption in a wireless communication scheme using PIC-microcontroller via zigbee channels," *Chaos, Solitons Fractals*, vol. 133, Apr. 2020, Art. no. 109646.

[8] A. Girdhar, H. Kapur, and V. Kumar, "A novel grayscale image encryption approach based on chaotic maps and image blocks," *Appl. Phys. B, Lasers Opt.*, vol. 127, no. 3, pp. 1–12, Mar. 2021.

[9] E. E.-D. Hemdan, "An efficient and robust watermarking approach based on single value decompression, multi-level DWT, and wavelet fusion with scrambled medical images," *Multimedia Tools Appl.*, vol. 80, no. 2, pp. 1749–1777, Jan. 2021.

[10] M. Nazari and M. Mehrabian, "A novel chaotic IWT-LSB blind watermarking approach with flexible capacity for secure transmission of authenticated medical images," *Multimedia Tools Appl.*, vol. 80, no. 7, pp. 10615–10655, Mar. 2021.

[11] *Data Encryption Standard (DES)*, Standard 46-3, FIPS, 1999.

[12] *Advanced Encryption Standard (AES)*, Standard 197, FIPS, 2001.

[13] C. L. Chowdhary, P. V. Patel, K. J. Kathrotia, M. Attique, K. Perumal, and M. F. Ijaz, "Analytical study of hybrid techniques for image encryption and decryption," *Sensors*, vol. 20, no. 18, p. 5162, Sep. 2020.

[14] Y. Bentoutou, E.-H. Bensikaddour, N. Taleb, and N. Bounoua, "An improved image encryption algorithm for satellite applications," *Adv. Space Res.*, vol. 66, no. 1, pp. 176–192, Jul. 2020.

[15] Y. Luo, X. Ouyang, J.-X. Liu, and L.-C. Cao, "An image encryption method based on elliptic curve ElGamal encryption and chaotic systems," *IEEE Access*, vol. 7, pp. 38507–38522, 2019.

[16] B. Deepan, C. Quan, Y. Wang, and C. J. Tay, "Multiple-image encryption by space multiplexing based on compressive sensing and the double-random phase-encoding technique," *Appl. Opt.*, vol. 53, no. 20, pp. 4539–4547, 2014.

[17] R. Enayatifar, A. H. Abdullah, and I. Isnin, "Chaos-based image encryption using a hybrid genetic algorithm and a DNA sequence," *Opt. Lasers Eng.*, vol. 56, pp. 83–93, May 2014.

[18] M. Kaur and V. Kumar, "Beta chaotic map based image encryption using genetic algorithm," *Int. J. Bifurcation Chaos*, vol. 28, no. 11, Oct. 2018, Art. no. 1850132.

[19] Q. Xu, K. Sun, C. Cao, and C. Zhu, "A fast image encryption algorithm based on compressive sensing and hyperchaotic map," *Opt. Lasers Eng.*, vol. 121, pp. 203–214, Oct. 2019.

[20] R. Matthews, "On the derivation of a 'chaotic' encryption algorithm," *Cryptologia*, vol. 13, no. 1, pp. 29–42, Jan. 1989.

[21] L. M. Pecora and T. L. Carroll, "Synchronization in chaotic systems," *Phys. Rev. Lett.*, vol. 64, no. 8, pp. 821–824, 1990.

[22] J. Fridrich, "Symmetric ciphers based on two-dimensional chaotic maps," *Int. J. Bifurcation Chaos*, vol. 8, no. 6, pp. 1259–1284, 1998.

[23] C. Pak and L. L. Huang, "A new color image encryption using combination of the 1D chaotic map," *Signal Process.*, vol. 138, pp. 129–137, Sep. 2017.

[24] H. Wang, D. Xiao, X. Chen, and H. Huang, "Cryptanalysis and enhancements of image encryption using combination of the 1D chaotic map," *Signal Process.*, vol. 144, pp. 444–452, Mar. 2018.

[25] A. Hasheminejad and M. J. Rostami, "A novel bit level multiphase algorithm for image encryption based on PWLCM chaotic map," *Optik*, vol. 184, pp. 205–213, May 2019.

[26] S. J. Sheela, K. V. Suresh, and D. Tandur, "Image encryption based on modified Henon map using hybrid chaotic shift transform," *Multimedia Tools Appl.*, vol. 77, no. 19, pp. 25223–25251, Oct. 2018.

[27] M. Ahmad, M. Z. Alam, S. Ansari, D. Lambić, and H. D. AlSharari, "Cryptanalysis of an image encryption algorithm based on PWLCM and inertial delayed neural network," *J. Intell. Fuzzy Syst.*, vol. 34, no. 3, pp. 1323–1332, 2018.

[28] H. Liu, A. Kadir, and J. Liu, "Color pathological image encryption algorithm using arithmetic over Galois field and coupled hyper chaotic system," *Opt. Lasers Eng.*, vol. 122, pp. 123–133, Nov. 2019.

[29] T. Gao, G. Chen, Z. Chen, and S. Cang, "The generation and circuit implementation of a new hyper-chaos based upon Lorenz system," *Phys. Lett. A*, vol. 361, nos. 1–2, pp. 78–86, Jan. 2007.

[30] T. M. Khlebodarova, V. V. Kogai, S. I. Fadeev, and V. A. Likhoshvai, "Chaos and hyperchaos in simple gene network with negative feedback and time delays," *J. Bioinf. Comput. Biol.*, vol. 15, no. 2, Apr. 2017, Art. no. 1650042.

[31] V. Basios and C. G. Antonopoulos, "Hyperchaos & labyrinth chaos: Revisiting Thomas–Rössler systems," *J. Theor. Biol.*, vol. 460, pp. 153–159, Jan. 2019.

[32] N. Balaska, Z. Ahmida, A. Belmeguenai, and S. Boumerdassi, "Image encryption using a combination of grain-128a algorithm and Zaslavsky chaotic map," *IET Image Process.*, vol. 14, no. 6, pp. 1120–1131, May 2020.

[33] T. Gao and Z. Chen, "A new image encryption algorithm based on hyper-chaos," *Phys. Lett. A*, vol. 372, no. 4, pp. 394–400, 2008.
[34] R. Rhouma and S. Belghith, "Cryptanalysis of a new image encryption algorithm based on hyper-chaos," *Phys. Lett. A*, vol. 372, no. 38, pp. 5973–5978, Sep. 2008.
[35] Z. Li, C. Peng, L. Li, and X. Zhu, "A novel plaintext-related image encryption scheme using hyper-chaotic system," *Nonlinear Dyn.*, vol. 94, no. 2, pp. 1319–1333, Oct. 2018.
[36] X. Chai, Z. Gan, and M. Zhang, "A fast chaos-based image encryption scheme with a novel plain image-related swapping block permutation and block diffusion," *Multimedia Tools Appl.*, vol. 76, no. 14, pp. 15561–15585, 2017.
[37] L. Liu, Y. Lei, and D. Wang, "A fast chaotic image encryption scheme with simultaneous permutation-diffusion operation," *IEEE Access*, vol. 8, pp. 27361–27374, 2020.
[38] H.-M. Yuan, Y. Liu, T. Lin, T. Hu, and L.-H. Gong, "A new parallel image cryptosystem based on 5D hyper-chaotic system," *Signal Process., Image Commun.*, vol. 52, pp. 87–96, Mar. 2017.
[39] Ü. Çavuşoğlu and S. Kaçar, "A novel parallel image encryption algorithm based on chaos," *Cluster Comput.*, vol. 22, no. 4, pp. 1211–1223, Dec. 2019.
[40] M. Zhou and C. Wang, "A novel image encryption scheme based on conservative hyperchaotic system and closed-loop diffusion between blocks," *Signal Process.*, vol. 171, Jun. 2020, Art. no. 107484, doi: 10.1016/j.sigpro.2020.107484.
[41] C.-F. Zhao and H.-P. Ren, "Image encryption based on hyper-chaotic multi-attractors," *Nonlinear Dyn.*, vol. 100, no. 1, pp. 679–698, Mar. 2020.
[42] L. O. Tresor and M. Sumbwanyambe, "A selective image encryption scheme based on 2D DWT, Henon map and 4D Qi hyper-chaos," *IEEE Access*, vol. 7, pp. 103463–103472, 2019.
[43] X. Gao, "Image encryption algorithm based on 2D hyperchaotic map," *Opt. Laser Technol.*, vol. 142, Oct. 2021, Art. no. 107252.
[44] M. D. Gupta and R. K. Chauhan, "Secure image encryption scheme using 4D-hyperchaotic systems based reconfigurable pseudo-random number generator and S-box," *Integration*, vol. 81, pp. 137–159, Nov. 2021.
[45] X. Wang and M. Zhao, "An image encryption algorithm based on hyperchaotic system and DNA coding," *Opt. Laser Technol.*, vol. 143, Nov. 2021, Art. no. 107316.
[46] X. Wang, S. Wang, Y. Zhang, and C. Luo, "A one-time pad color image cryptosystem based on SHA-3 and multiple chaotic systems," *Opt. Lasers Eng.*, vol. 103, pp. 1–8, Apr. 2018.
[47] S. Rajendran, K. Krithivasan, M. Doraipandian, and X.-Z. Gao, "Fast preprocessing hex chaos triggered color image cryptosystem," *Multimedia Tools Appl.*, vol. 79, no. 7, pp. 1–23, 2020.
[48] S. Zhou, X. Wang, Z. Wang, and C. Zhang, "A novel method based on the pseudo-orbits to calculate the largest Lyapunov exponent from chaotic equations," *Chaos, Interdiscipl. J. Nonlinear Sci.*, vol. 29, no. 3, Mar. 2019, Art. no. 033125.
[49] M. Ghebleh, A. Kanso, and D. Stevanović, "A novel image encryption algorithm based on piecewise linear chaotic maps and least squares approximation," *Multimedia Tools Appl.*, vol. 77, no. 6, pp. 7305–7326, Mar. 2018.
[50] M. J. Rostami, A. Shahba, S. Saryazdi, and H. Nezamabadi-Pour, "A novel parallel image encryption with chaotic windows based on logistic map," *Comput. Electr. Eng.*, vol. 62, pp. 384–400, Aug. 2017.
[51] S. Zhou and X. Wang, "Identifying the linear region based on machine learning to calculate the largest Lyapunov exponent from chaotic time series," *Chaos, Interdiscipl. J. Nonlinear Sci.*, vol. 28, no. 12, Dec. 2018, Art. no. 123118.
[52] Intel. (Jun. 8, 2021). *Architecture Instruction Set Extensions Programming Reference*. Version 319433-044. [Online]. Available: https://software.intel.com/content/www/us/en/develop/download/intel-architecture-instruction-set-extensions-programming-reference.html
[53] C. R. Harris, K. J. Millman, S. J. van der Walt, R. Gommers, P. Virtanen, D. Cournapeau, E. Wieser, J. Taylor, S. Berg, N. J. Smith, and R. Kern, "Array programming with numpy," *Nature*, vol. 585, no. 7825, pp. 357–362, 2020.
[54] M. Gataric, G. S. D. Gordon, F. Renna, A. G. C. P. Ramos, M. P. Alcolea, and S. E. Bohndiek, "Reconstruction of optical vector-fields with applications in endoscopic imaging," *IEEE Trans. Med. Imag.*, vol. 38, no. 4, pp. 955–967, Apr. 2019.
[55] G. W. Allan. (Feb. 3, 2018). *The USC-SIPI Image Database*. Version 6. [Online]. Available: https://sipi.usc.edu/database/SIPI_Database.pdf

BIN GE received the Ph.D. degree in engineering from the University of Chinese Academy of Sciences, in 2016. He is currently a Lecturer with Nantong Vocational University. His current research interests include the theory and application of cryptography and chaotic cryptography.

XU CHEN received the Ph.D. degree in engineering from the Institute of Semiconductors, CAS, in 2005. She is currently an Associate Researcher with the Institute of Semiconductors, CAS. Her current research interests include image processing, artificial intelligence, and pattern recognition.

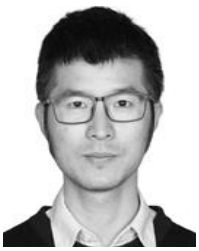

GANG CHEN received the Ph.D. degree in engineering from the University of CAS, in 2013. He is currently an Associate Researcher with the Institute of Semiconductors, CAS. His current research interests include image processing and artificial intelligence.

ZHIHUA SHEN received the Ph.D. degree in engineering from Xi'an Jiao Tong University, in 2017. He is currently a Lecturer with Nantong Vocational University. His current research interests include chaos theory and circuit design.